A Holocene alpine seismic chronicle from Lake Aiguebelette (NW French Alps)

Mathilde Banjan[1,2], Christian Crouzet[1], Hervé Jomard[2], Pierre Sabatier[3], David Marsan[1], Erwan Messager[3]

[1]Université Savoie Mont Blanc, Université Grenoble Alpes, CNRS, IRD, Université Gustave Eiffel, ISTerre, Le Bourget du lac, France
[2]IRSN - Bureau d'évaluation des risques sismiques pour la sûreté des installations, Fontenay-aux-Roses, France
[3]Université Savoie Mont Blanc, CNRS, EDYTEM, Le Bourget du lac, France

Correspondence to: Christian Crouzet (christian.crouzet@univ-smb.fr) and Mathilde Banjan (mathilde.banjan@gmail.com)

Abstract. Lake sediments are valuable archives and can help construct a chronology of event deposits induced by seismic events. Such a chronology can be used to better understand the recurrence times between seismic events over longer periods than those covered by historical seismicity catalogs. However, only a few studies in lake palaeoseismology have focused on areas with moderate seismicity. This study aims to improve the catalog of paleoseismological archives in the front of the Western Alps. In this part, new multi-proxy data from the sedimentary archives of Lake Aiguebelette (France) allow the identification of 32 homogenites (thickness ≥ 0.5 cm) interpreted as of coseismic origin over the Holocene. An age model based on short-lived radionuclides, paleomagnetic data and radiocarbon ages constrains the chronology of sedimentary deposits in the deep basin of Lake Aiguebelette.

Among these homogenites, several were deposited at time intervals compatible with historical seismic events. To identify the historical seismic events likely to have generated the event deposits identified in the sedimentary sequences of the deep basin of Lake Aiguebelette, the Earthquake Sensitivity Threshold Index (ESTI) method is used. Historical seismicity catalogs with uncertainties about intensities and epicenter coordinates for earthquakes make correlations to event deposits difficult. To better understand which seismic events may have been archived, a relative comparison was conducted between the pseudospectral acceleration (PSA) values calculated for each event in the FCAT-17 seismic catalog for two distinct frequencies.

Based on this PSA approach, for higher frequencies (5 Hz), the contribution of nearby and moderate events is significantly stronger than that of strong and distant events in the lake sequence of Aiguebelette. Thus, the chronicle established based

31   on the event deposits archived in Lake Aiguebelette sediment is interpreted as representative of local events (epicentral

32   distance to the lake < 50 km). Recurrence intervals between the deposition of event layers do not follow a specific

33   distribution (log-normal, Weibull, gamma or exponential) but might be a combination of several distributions. This

34   suggests possible coexistence of several processes over the Holocene, impacting the evolution of the seismicity in this

35   area.

1 Introduction

37   In stable continental regions, characterised by low to moderate seismicity, there are very few historical records of large

38   earthquakes, as the time interval between strong seismic events is often greater than the period covered by seismic catalogs

39   (Cara et al., 2015). In such areas, palaeoseismic data covering a long period of time are then essential for constructing a

40   comprehensive long-term seismic chronicle and understanding seismic cycles of a given region.

41   In recent decades, it has been demonstrated that sediments are valuable archives for reconstructing seismic chronicles in

42   both marine (e.g. Nakajima and Kanai, 2000; Beck et al., 2007) and lacustrine environments (e.g. Strasser et al., 2013;

43   Moernaut et al., 2014). These sediment archives can span from historical times to longer periods. In the french Alps where

44   this study focuses, few sedimentary archives that cover the entire Holocene time span are available (only Annecy – Beck et

45   al., 1996; La Thuile and Aiguebelette (Banjan et al., 2023) lakes record the entire Holocene). At the scale of the entire

46   alpine belt, the construction of long-term seismic chronicles is still challenging (see for example Beck et al., 1996;

47   Wilhelm et al., 2016; Strasser et al., 2013; Rapuc et al., 2018; Bellwald et al., 2024 Banjan et al., 2023).

48   To build a seismic chronicle based on sediment archives, a mandatory step is to demonstrate that event layer deposition

49   is related to a seismically induced process (Sabatier et al., 2022), in general by using comparison with historical seismicity

50   (Chapron et al., 1999; Strasser et al., 2006; Wilhelm et al., 2016; Kremer et al., 2017). However, lacustrine

51   palaeoseismological studies often focus on active geodynamic contexts where the occurrence of major earthquakes with

52   magnitudes typically exceeding Mw 7 is common (Moernaut et al., 2011; 2018; 2020; Gastineau et al., 2021). Only a few

53   seismic chronicles have been established for areas of moderate seismicity in the available literature (Kremer et al., 2015;

54   2017; Daxer et al., 2022). The main difficulty in those regions lies in the fact that earthquake ground motions commonly

55   associated with moderate earthquakes are often very close to the sensitivity limit of lake sediments to record seismically

56   induced destabilisation. If we take the example of macroseismic intensities, classically used to quantify the severity of

57   ground motions for historical earthquakes, it is generally considered that it should be of the order of VI to VII (in EMS98

58   or MSK64 macroseismic scales) in lacustrine environments to be recorded by the lake sediments, particularly in the Alps

59   (Strasser et al., 2013; Petersen et al., 2014; Kremer et al., 2015; Wilhelm et al., 2016).

[handwritten note: Some missing References of Alpine lake studies: - Oswald - Daxer]

60   In addition, several studies based on different lake sedimentary sequences show that the possibility of a given earthquake

61   at a given distance to be recorded in a lake varies in the same region (Wilhelm et al., 2016). This variability between lake

62   sequences shows a different sensitivity to seismically induced instabilities (Moernaut et al., 2014; Van Daele et al., 2015;

63   Wilhelm et al., 2016) and is interpreted as mainly related to the sedimentation rate, linked to slope recharge capabilities *[handwritten note: → What about surficial remobilisation?]*

64   (Wilhelm et al., 2016). Moreover, in a given lake system if the sedimentation rate change, it could lead to a

65   misinterpretation in seismic cycles due to a period with a better ability to record an earthquake with higher sedimentation

66   rate (Rapuc et al., 2018; Gastineau et al., 2021).   *[handwritten note: higher sensitivity]*

67

68   The aims of this work are to (1) better understand perialpine lakes sensitivity to earthquake shaking in a moderately active

69   seismotectonic region and (2) improve the Holocene palaeoseismic catalog in the NW Alps. These objectives are studied

70   through the case of Lake Aiguebelette. This lake is selected as a unique palaeoseismological archive in the region with

71   little to no flood record and finely laminated sediments, which is not the case for neighbouring lakes (Chapron et al.,

72   1999; Nomade, 2005; Wilhelm et al., 2013; Bajard et al., 2016).

73   **2 Regional Settings**

74   The study site is located at the border between the NW Alps and the Jura Mountains (Fig. 1). In this area, Lake

75   Aiguebelette is a postglacial perialpine lake located 373 meters above sea level. The main tributary (Leysse de Novalaise)

76   enters the northern part of the lake (Fig. 2). The catchment area of the lake (~70 km^2) is characterised by steep slopes of

77   the "Chaîne de l'Epine" (Fig. 2), covered by forests on its eastern side, and flatter grasslands on its western side. The

78   main lithologies and sediment sources in the watershed are Jurassic and Cretaceous limestones on the eastern flank and

79   Neogene sandy molasses and Quaternary Würmian tills on the western side (Messager et al., 2022; Fudral et al., in press;

80   Banjan et al., 2023). The lake's morphology consists of three subbasins with depths reaching up to 45 m in the northern

81   basin, 71 m in the southeastern basin and 29 m in the southwestern basin (Fig. 2). Small islets separate the shallow and

82   deep southern basins.

83   The study area is located in a moderately active seismotectonic zone. However, several active faults have been evidenced

84   in the studied area, such as the Col du Chat, Culoz and Vuache faults (Fig. 1), (Baize et al., 2011; de la Taille et al., 2015;

85   Jomard et al., 2017). From the FCAT-17 earthquake catalogue (Manchuel et al., 2018), the more significant historical and

86   instrumental earthquakes in the area are the 1784 CE event (Mw 4,9±0.3) with an unknown seismogenic source, the 1822

87   CE Bugey earthquake (Mw=5.5±0.4), which most probably occurred along the Culoz fault, and the 1996 CE Epagny

88   earthquake (Mw=4.7±0.2), triggered along the Vuache fault.
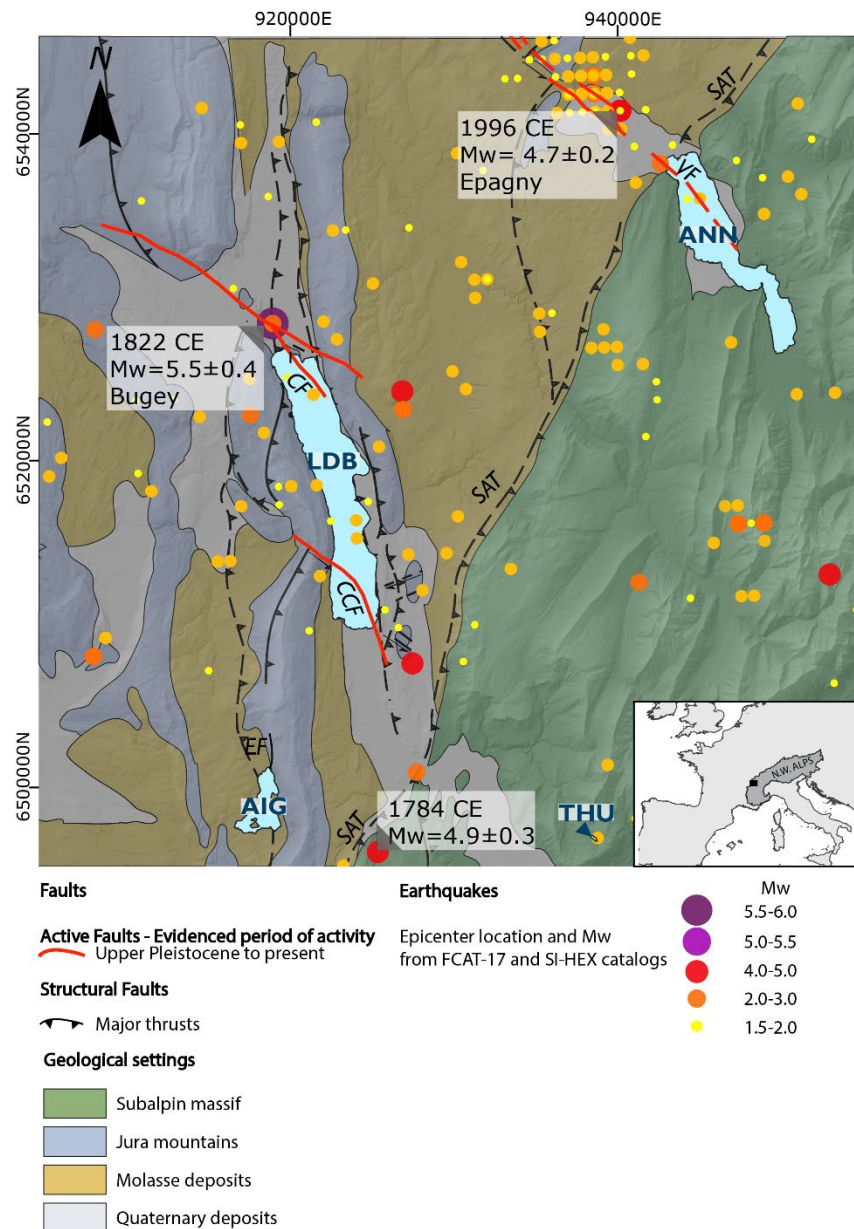
Fig. 1: Seismicity map of the NW Alps at the border with the French Jura Mountains. Epicentre locations and magnitudes are based on the FCAT-17 and SI-HEX databases (Cara et al., 2015; Manchuel et al., 2018). The main active faults from the Upper Pleistocene are presented in red (CF: Culoz Fault; CCF: Col Du Chat Fault; VF: Vuache Fault). Lake Aiguebelette (AIG), Annecy (ANN), Bourget (LDB) and La Thuile (THU) are presented in light blue. The geological settings are from the BRGM 1/50000 regional map and C. Crouzet personal communications. Projection: Lambert-93 (EPSG 2154).

89 .

95 3 Methods

96 3.1 Coring

[handwritten annotation: Why do you not consider the other cores?]

97   In Lake Aiguebelette, a total of 65 cores were retrieved through several campaigns using a Uwitec platform and corers.

98   Five cores from the southern basin are meaningful to this study (Fig. 2), including a ~16 m-long sediment sequence,

99   AIG17III (45.55043; 5.80144; at a water depth of ca 70 m; IGSN: TOAE0000000393 to TOAE000000410), and four

100   pilot cores, AIG20-01 (45.55081; 5.80107; at a water depth of ca. 70.6 m; ISGN: TOAE0000000325), AIG16-08

101   (45.5506; 5.80128; at a water depth of ca. 72.8 m; ISGN: TOAE0000000168), AIG16-06 (45.55080; 5.80281; at a water

102   depth of ca. 73.6 m; ISGN: TOAE0000000166) and AIG16-05 (45.55075; 5.80295; at a water depth of 73.7 m; ISGN:

103   TOAE0000000165). *[handwritten annotation: → coordinates miss N and E labels, and the IGSN numbers would probably better fit in a table in SI]*

104   For the long sequence (AIG17III), the sediment was retrieved from three parallel holes (with a 70 cm depth offset between

105   them to ensure large section overlaps) using 2 m long core liners 90 mm in diameter with a piston corer. For the three

106   pilot cores, 2 m long core liners of 63 mm in diameter were used with a gravity corer and hammering.

107

108
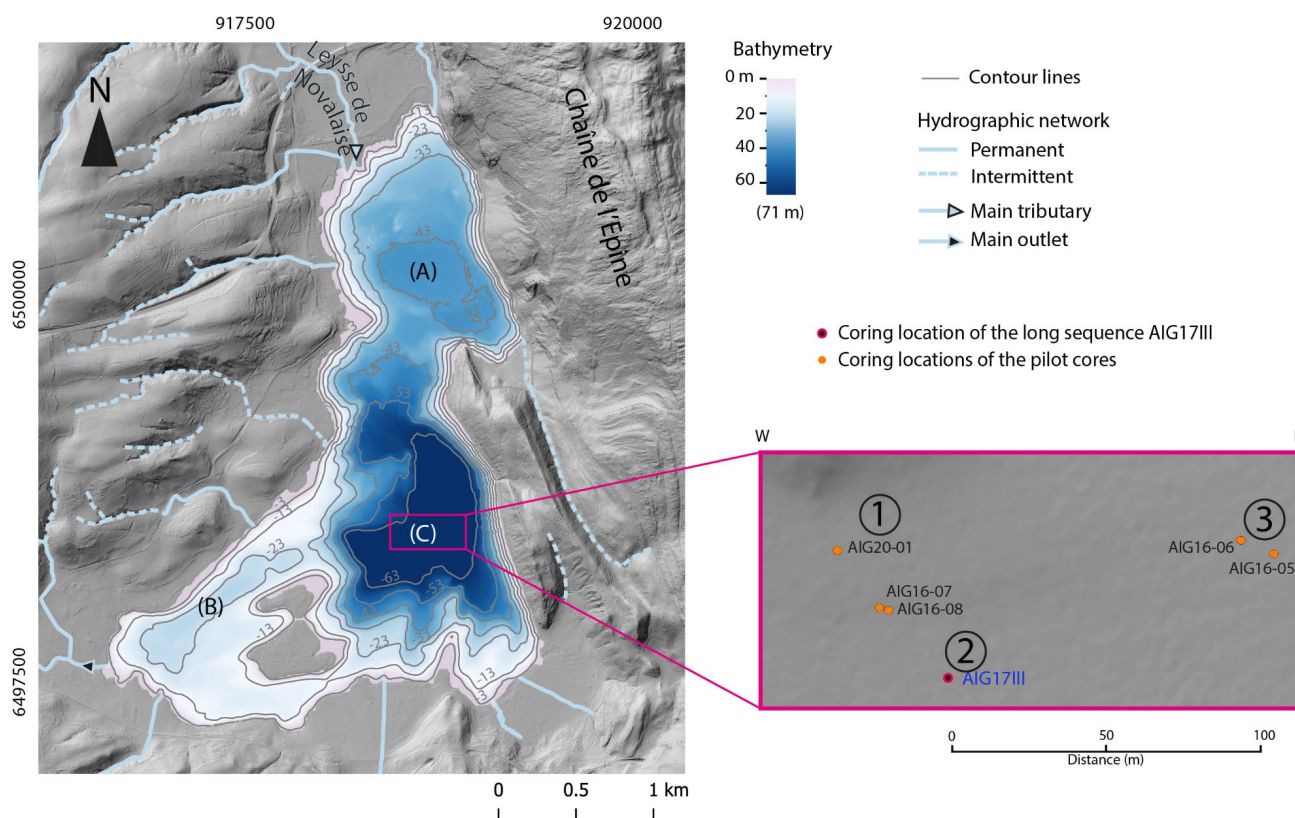
Fig. 2: Map of Lake Aiguebelette with a zoom on the deepest southern basin displaying core locations (AIG20-01, AIG17III, AIG06-05, AIG16-06, AIG16-07 and AIG16-08). Sequences AIG16-07 and AIG16-08 are available in the Supplementary Material section SM-2. (A), (B) and (C) indicate the location of the deepest point for each of the three subasin, respectively 45, 29 and 71 m depth. Projection: Lambert-93 (EPSG 2154)

3.2 Sedimentology

The studied cores were split into two halves, and one of each half section was described in detail and photographed. The different sedimentary facies were first described and identified with the same visual criteria used in a previous study to build the long sequence AIG17III (Banjan et al., 2023). These criteria are helpful in the visual characterization of event layers interbedded in continuous sedimentation. The sediment logs are provided in the supplementary materials (SM-1). Grain-size analyses were performed with a Beckman Coulter Life Science 13230 XR laser particle-size analyser (EDYTEM Laboratory). A 5 mm sampling step was selected along the Holocene event layers (thickness ≥ 5 mm) of the AIG 16-05 and AIG 17III. For the continuous sedimentation, a 2 to 5 cm sampling step was used.

123 Five of the cores displayed in Fig. 2 are key materials to sedimentological analysis as follow: AIG20-01 for radioelement

124 dating; core AIG16-08 for radiocarbon dating and correlations with core AIG17III that is the only core that covers the

125 entire Holocene period, and finally cores AIG16-06 and AIG16-05, bearing the most recent event layers.

126

3.3 Geochemistry

128 X-ray fluorescence (XRF) analyses were performed on the sediment surface of the split cores at 5-mm intervals with an

129 Avaatech core scanner (EDYTEM laboratory). Relative geochemical compositions were obtained for different settings in

130 measurement runs (1) and (2) as follows: (1) 10 kV and 0.1 mA for 30 s to detect lightweight elements such as Al, Si, P,

131 K, Ca, Ti, Mn, and Fe; (2) 30 kV and 0.3 mA for 30 s to detect heavier elements Br, Rb, Sr, Zr and Pb. To avoid dilution

132 effects due to water and the influence of the sediment matrix, the relative abundances of elements are expressed as log-

133 ratios (Weltje et al., 2015).

You should use centered log ratios.

134 A Vega3 Tescan Scanning Electron Microscope (SEM) was used on a sediment thin section representative of laminated

135 facies. To map chemical elements and examine the elemental composition of precise areas on the sediment thin section,

136 further analyses were conducted with an energy-dispersive spectroscopy (EDS) probe (Rayspec and SamX electronic

137 system and software). An 8 cm long sediment slab sampled in the AIG17III sequence and representative of the laminated

138 facies was resin-embedded to make a 1 mm thick thin section for microscopic observation and chemical analyses.

139 *- Better to move this upfront*

3.4 Magnetic and palaeomagnetic investigations

141 Magnetic measurements and analyses were performed at the CEREGE laboratory (Aix-Marseille University). U-channels

142 were sampled from the AIG17III, AIG20-01 and AIG16-05 sedimentary cores.

143 First, the U-channels were exposed to a stepwise alternating field (AF) to progressively demagnetize the Natural

144 Remanent Magnetization (NRM) with steps of 10 mT until the remanence passed a threshold (equivalent to 20% of the

145 NRM) or until the maximum capacity of the measuring instrument. The magnetization was measured before any treatment

146 and after each AF treatment using a superconducting quantum interference device (SQUID) through a cryogenic

147 magnetometer (2G 760R) located in a shielded room. The NRM data were analysed with demagnetization curves and

148 principal component analyses (Puffin Plot software) (Lurcock and Wilson, 2012), to establish Characteristic Remanent

149 Magnetization (ChRM) curve versus depth.

the

150   Isothermal Remanent Magnetization (IRM) was created by successively passing the U-channels through Halbach rings

151   imparting 0.3 T and 0.6 T magnetic fields. The field induced by the magnetized sediment was measured after each

152   application of the field with a high-resolution magnetic scanner (Demory et al., 2019).

153   To determine the anisotropy of magnetic susceptibility (AMS), cubic samples were collected from the event layers (with

154   a thickness $\geq$ 2 cm) and surrounding sediment of the AIG17III sequence in 8 cm^3 nonmagnetic plastic boxes. The

155   measurements were conducted with a magnetic susceptibility meter MFK1 (AGICO) to determine the susceptibility tensor

156   that can be represented by an ellipsoid with three eigenvectors (Kmax, Kint and Kmin). The AMS ellipsoid is assumed

157   to reflect the preferred orientation of particles in the sediments. The magnetic foliation $F = K_{int}/K_{min}$ has been used to

158   characterize homogenite-type deposits (Campos et al., 2013; Rapuc et al., 2018; Banjan et al., 2023).

↳ also Vermassen et al 2023?

159   **3.5 Time constraints on the sediments**

160   A previous age-depth model for the AIG17III sequence was published in Banjan et al. (2023) based on only nineteen

161   radiocarbon dating. Here we add new constraints (SM-3, SM-4) derived from short-lived radioelements, varve counting

162   and palaeomagnetic data. A comparison was performed between ChRM data (inclination, declination) and continuous

163   global geomagnetic field models such as discussed in Crouzet et al. (2019a). The Serac R package is used to create an

164   age model from short-lived radionuclides (Bruel and Sabatier, 2020). The new age-depth model was calculated with the

165   use of the clam R package (Blaauw, 2010). It is important to remember that the age depth model has to take into account

166   an event-free composite depth, event layers being interpreted as instantaneous deposits (Sabatier et al., 2022).

↳ Why not the more commonly used Bacon ?

167   **4 Results and interpretations**

168   **4.1 Sediment facies in Lake Aiguebelette**

169   In the deep basin of the lake, 8 sediment units were defined in the 16-meter-long core AIG17III (Banjan et al., 2023;

170   entire sequence description available in SM-1). These units mainly consist of brown-greenish and grayish clayey to silty

171   sediments. Some units are characterized by alternation of distinct laminae (units 1, 3, 4, 6, and 8), while others are

172   characterized by faint laminations (units 2, 5, and 7).

→ Repetition? Or another sequence?

173   In this sequence as well as in the pilot cores, sediments mainly consist of clayey to silty laminations. Millimetre-scale

174   laminations are visible and consist of the repetition/alternation of triplets of laminae, identified through SEM analyses

175   and geochemical cartography. One triplet is composed of (1) a dark Al- and Ti-rich (dark-gray to brown) lamina, (2) an

176   olive to gray Si-rich lamina and (3) a clear Ca-rich (white) lamina (Fig. 3).

177   Diatoms have been observed in the Si-rich lamina that can be interpreted as a seasonal spring deposit such as in other

178   alpine lakes, whereas the Ca-rich lamina is related to carbonate bio-induced precipitation in late spring to summer and

179   the Al-rich lamina can be interpreted as a fall/winter deposit with more detrital input (Giguet-Covex et al., 2010; Wirth

180   et al., 2013).

181   These background sediments are intermittently interbedded with event layers of different thicknesses (millimetric to

182   pluricentimetric) (SM-2, SM-5). These event layers are identified visually, and for those that are sufficiently thick,

183   typically $\geqslant 0.5$ cm, it is possible to recognize facies such as turbidites (Tu, poorly sorted normal graded deposit),

184   homogenites (Hm, homogeneous clayey sediment topped by a clay cap) or the succession of both (Tu+Hm), (Ambraseys

185   and Finkel, 1991; Campos et al., 2013; de Gelder et al., 2022; Banjan et al., 2023).
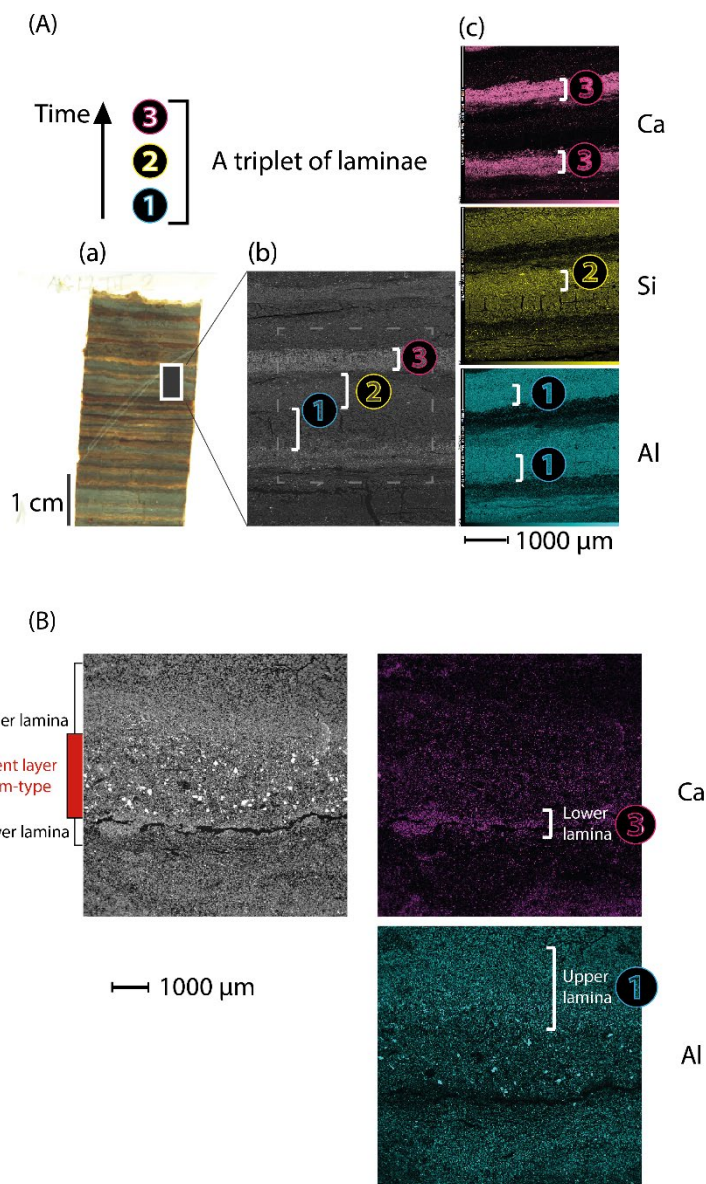
Fig. 3: (A) AIG17III sediment thin section and SEM observation of the background lamination. (a) Thin section with laminae triplets visible to the naked eye; (b) SEM image of a few selected laminae (magnification x50); (c) geochemical cartographies: Al in blue, Si in yellow and Ca in pink (magnification x79; high tension 16 kV). (B) AIG16-05 sediment SEM observation focused on the Hm-type event layer deposited between 1760 and 1824 cal CE. The laminae under the base (lower lamina) and at the top (upper lamina) of the event layer are displayed. Al is in blue, and Ca is in pink. (Magnification x34; high tension 10 kV). The laminae can be associated with a season (the Al-rich lamina can be interpreted as a winter varve, while the Ca-rich lamina can be interpreted as a summer varve).

[handwritten annotation: You should first describe your updated age model]

194

4.2 Event deposit characterization

196

197 The first step of event deposit characterization is based on the visual observation of the studied cores. Tu+Hm and Hm

198 facies are identified as mentioned in the previous section. In cores AIG16-05 and AIG16-06, seven event layers are

199 visually identified in the top 100 cm, the four upper event layers (total thickness of 32 mm for the four deposits) are

[handwritten annotation: ? You mean no background? So stacked/amalgamated deposits? Check terminology!]

200 successively deposited, which is a unique case in the overall dataset. In the AIG17III long sediment sequence (16 m long),

201 a total of 62 event layers are visually identified, regardless of thickness, including 55 event layers during the Holocene.

202 In this sequence (AIG17III), 32 event layers have a thickness ≥0.5 cm. Among them, the youngest is archived at 161 cm

203 (master core depth). In this section, the results of measurements used to characterize event deposits are presented, in

204 particular using the example of the thickest event layer (4.8 cm-thick) observed in the top 5 m of the long deep basin

205 sediment sequence (Fig. 4). This event layer ~~deposit~~ consists of a silty brown-olive homogeneous sediment with a clear

206 millimetric clay cap, visually interpreted as a homogenite (Hm). As previously demonstrated by Campos et al. (2013),

207 sometimes, the Hm deposit is subdivided into a "lower homogenite", corresponding to a settling phase under the seiche

208 effect, and an "upper homogenite", corresponding to a settling phase of stable suspension (these facies can be identified

209 through magnetic (AMS foliation) and grain-size data (Campos et al., 2013)). In the studied deposit, the grain size of the

210 continuous background sediment preceding the event layer has a D90 mean of 21.58 µm (with values ranging between

211 17 µm <D90< 25 µm) and a σ_{SC_D90} = 1.87 µm. Within the Hm facies, two parts can be identified: 1-, a lower part (lHm)

212 with a D90 mean of 54.9 µm (values ranging between 46.8 µm <D90< 64.1 µm) and σ_{lHm_D90}= 6.5 µm and 2-, an upper

213 part (uHm) with a D90 mean of 39.8 µm (values ranging between 34 µm <D90< 43 µm), with σ_{uHm_D90}=3.4 µm (Fig. 4).

214 The whole Hm facies is slightly coarser than the background sediment facies. Within the Hm facies, lHm is coarser than

215 uHm, certainly due to different settling phases of the sediment, as explained in Campos et al. (2013). The logarithmic

216 ratio of Ca/Ti is lower in the event layer than in the background sediment (Fig. 4), suggesting either a different source for

217 the event layer sediment *or* remobilized before deposition with higher Ti content (possibly the remobilization of sediment

218 on unstable slopes).

219 The anisotropy of magnetic susceptibility foliation (F) measured in the background sediment and in the graded base of

220 the event layer is <1.01, whereas it is ≥1.02 in the Hm facies (Fig. 4). IRM data show values ≤0.38 µT in the event layer

221 (with the lowest values at depth corresponding to the Hm facies, similar to the Hm in the 115 cm-thick event layer of the

222 same sequence, which was previously interpreted as seismically induced (Banjan et al., 2023)). This high AMS foliation

223 criterion, which brings the highest level of confidence to interpret event deposit as seismically induced, can only be

[handwritten annotation: not clear what you mean here. Which Hm, which 'same sequence', which MS on event deposit?]

[handwritten annotation: Why? ↳ discussion!]

224 established on Hm deposits with a thickness ⩾2 cm and observed in Figure 4. This thickness limitation is due to the

225 sensitivity of measurement device that need 8 cm³ of material sampled in 2*2*2 plastic cubes.

226 *should go in methods section*

227 To characterize the event layers with thicknesses ranging between 0.5 and 2 cm, it is possible to compare their grain-size

228 distribution in a Passega chart (Passega, 1964), with that of Hm and Tu+Hm deposits ⩾2 cm (and previously characterized

229 by a high AMS foliation). If they are all following the same trend, it is possible to interpret the thinner deposits as induced

230 by the same process than the thicker ones. In this study, grain-size data acquired on all the event layers with a thickness

231 > 0.5 cm and visually interpreted as homogenites or turbidite-homogenites are aligned and follow the same trend (Fig. 5),

232 which suggest a shared depositional mechanism (Wilhelm et al., 2013).

233
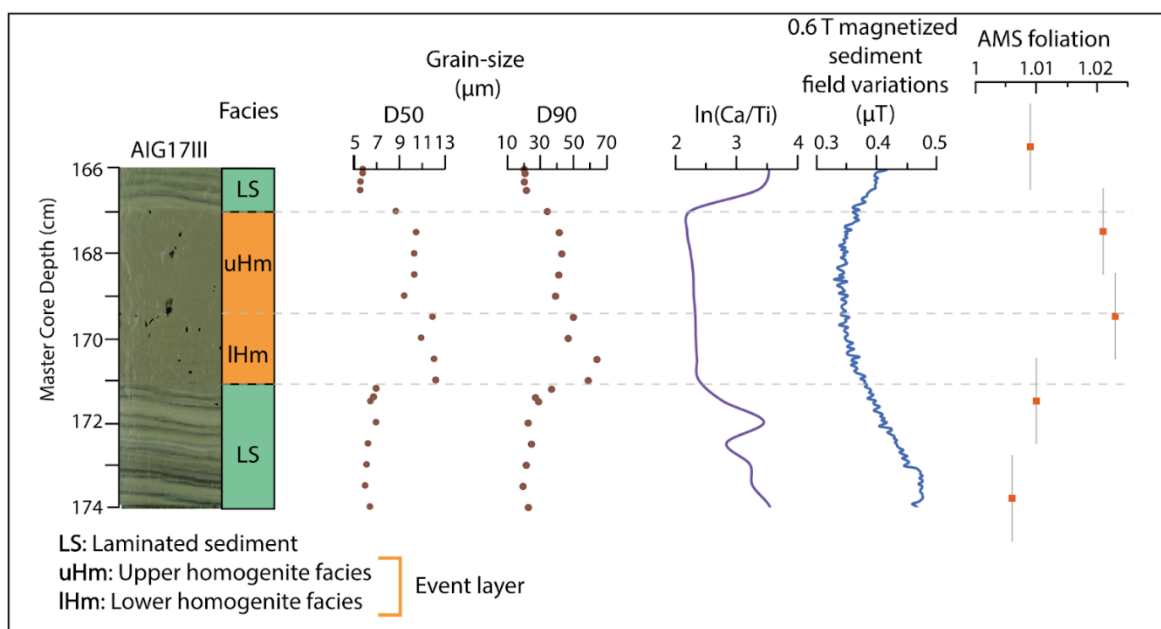
234
235 **Fig. 4: Main sedimentological, geochemical and magnetic results for a thick event layer present between 167.5 and 171 cm in**
236 **the AIG17III sequence. From left to right, data are presented versus MCD depth (cm): photography and identification of the**
237 **different facies; grain-size measurements, with D50 and D90 values (µm); geochemical ln ratio (Ca/Ti); magnetic field**
238 **variations induced by the magnetized sediment (equivalent to low isothermal remanent magnetization, Demory et al., 2019);**
239 **Anisotropy of Magnetic Susceptibility (AMS) foliation.**

240

241
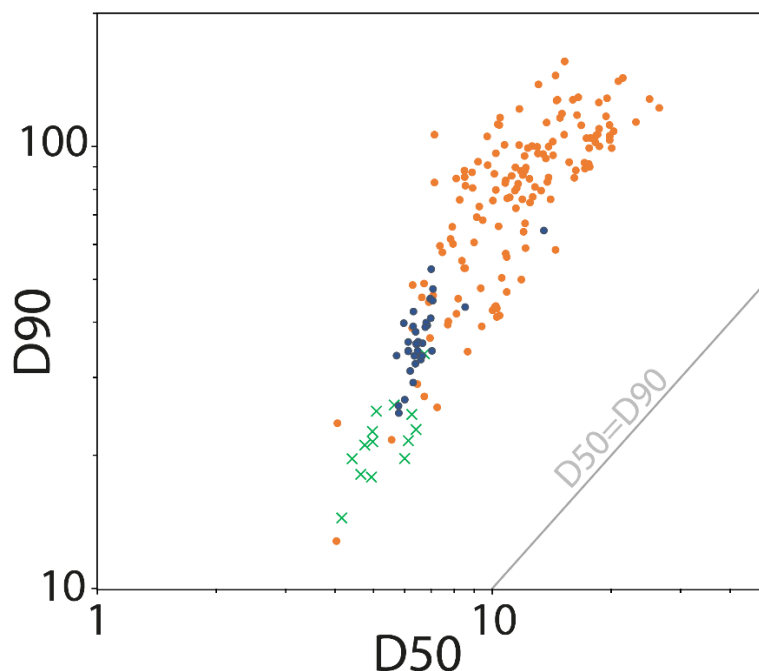
Fig. 5: Passega-type diagram (D90 vs. D50 and logarithmic sorting vs. D50). Orange dots: grain-size data of 26 event layers thicker than 0.5 cm from the AIG16-05 and AIG17III sequences (interpreted as Hm or Tu+Hm deposits). Blue dots: grain-size data of the homogenite constituting the thickest event layer of the deep basin sequence, presented in Banjan et al. (2023) and interpreted as seismically induced. Green crosses: grain-size data of the Holocene background sediment.

4.3 Core-to-core correlations

Core-to-core correlations were first established visually, with the use of laminae succession and the color and thickness of a specific deposit that stands out in both cores. Single XRF element (Ca and K) variations along the cores were also used to confirm the first correlations. In the same way, additional correlations were made possible with the use of IRM data (Fig. 6).

To estimate the depositional age range for each event layer of the AIG16-05 sequence, core-to-core correlations were made with the deep basin long sequence (AIG17III) (Fig. 6).

Four event layers are correlated between the two sequences (AIG16-05 and AIG17III). This enables us to constrain the chronology of the AIG16-05 sequence and to improve the count of the event layers deposited during the historical period (Table 1).

259

Depositional age range (yr CE)	Base (MCD depth)	Top (MCD depth)	Thickness (cm)	Correlated to AIG 17III
1921-1929 (*)	16.1	13.5	2.6	no
1760-1824	40	39.2	0.8	no
1528-1586	82.5	82.3	0.2	no
1581-1647	90	89.3	0.7	no
1327-1372	128	127.5	0.5	no
1186-1256	144.5	140.5	4	yes
1039-1127	163.8	163.2	0.6	yes
945-1033	177.8	177.2	0.6	no
712-801	208.6	205.8	2.8	yes
630-729	218.2	217.2	1	yes

260

261 **Table 1: Identification of event layers in the AIG16-05 sequence (depth), estimated time of deposition based on radiocarbon**
262 **ages and correlations with the AIG17III sequence. The "yes" mention in the last column indicate the event layers that have**
263 **been identified in both the AIG16-05 and AIG17III sequences. (*): 4 successive event layers**
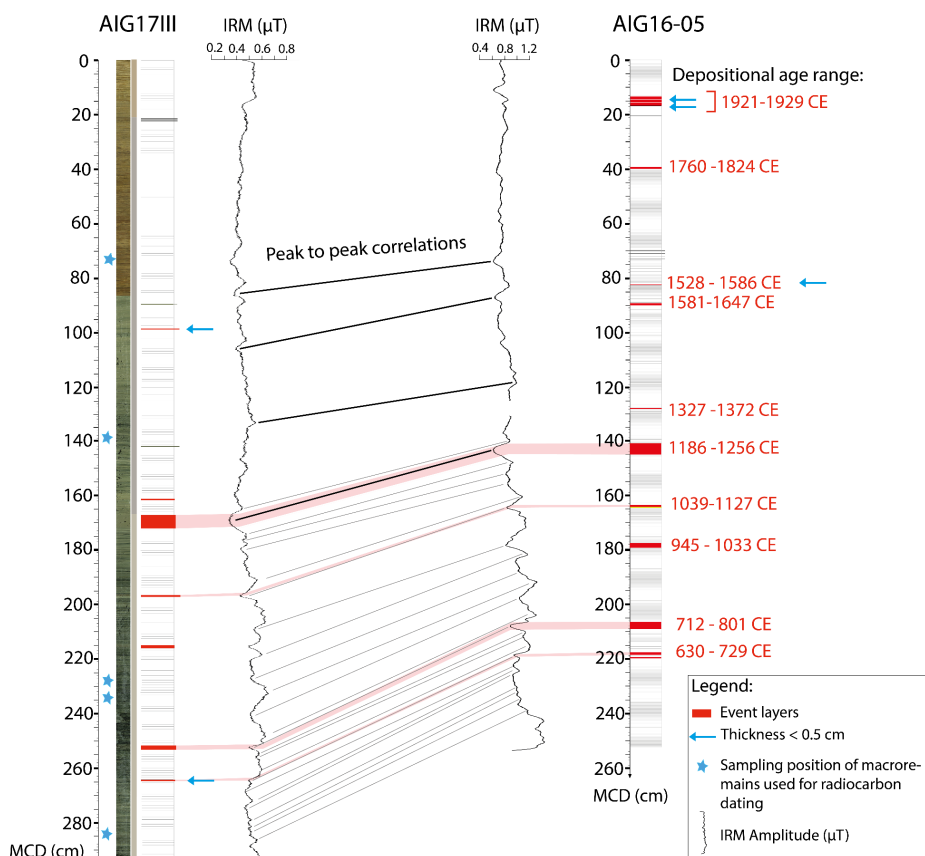
Fig. 6: Core-to-core correlation between AIG17III and AIG16-05 sequences based on IRM data. Depositional age ranges are given in red next to each event layer of the sediment sequence AIG16-05. These ages are derived from the age-depth model presented in Fig. III-8. The event layers are represented by red rectangles, and those with a thickness < 0.5 cm are indicated by a blue arrow.

4.4 Synthetic age depth model

4.4.1 Radioelements

The ^{210}Pb in excess is plotted downcore on a logarithmic scale. A CFCS (Constant Flux Constant Sedimentation) model based on the R package serac was used to calculate the ages continuously along the core depth (Bruel and Sabatier, 2020). The mean sedimentation rates are estimated at 2.1 mm.yr^{-1} for the upper 18 cm (Fig. 7). The ^{137}Cs downcore profiles present an upper peak at 5.5 cm, which corresponds to the 1986 CE Chernobyl accident (C 1986 in Fig. 7), and a lower

276   peak at 10.5 cm, which corresponds to the maximum of the Nuclear Weapon Tests (NWT) in the Northern Hemisphere

277   in 1963 CE (NWT 1963 in Fig. 7). The last interpretation is confirmed by a peak of ^{241}Am activities, which corresponds

278   to the NWT (Appleby et al., 1991). The first augmentation of ^{137}Cs is observed at 13.5 cm and corresponds to 1955 CE

279   (Bruel and Sabatier, 2020).

280
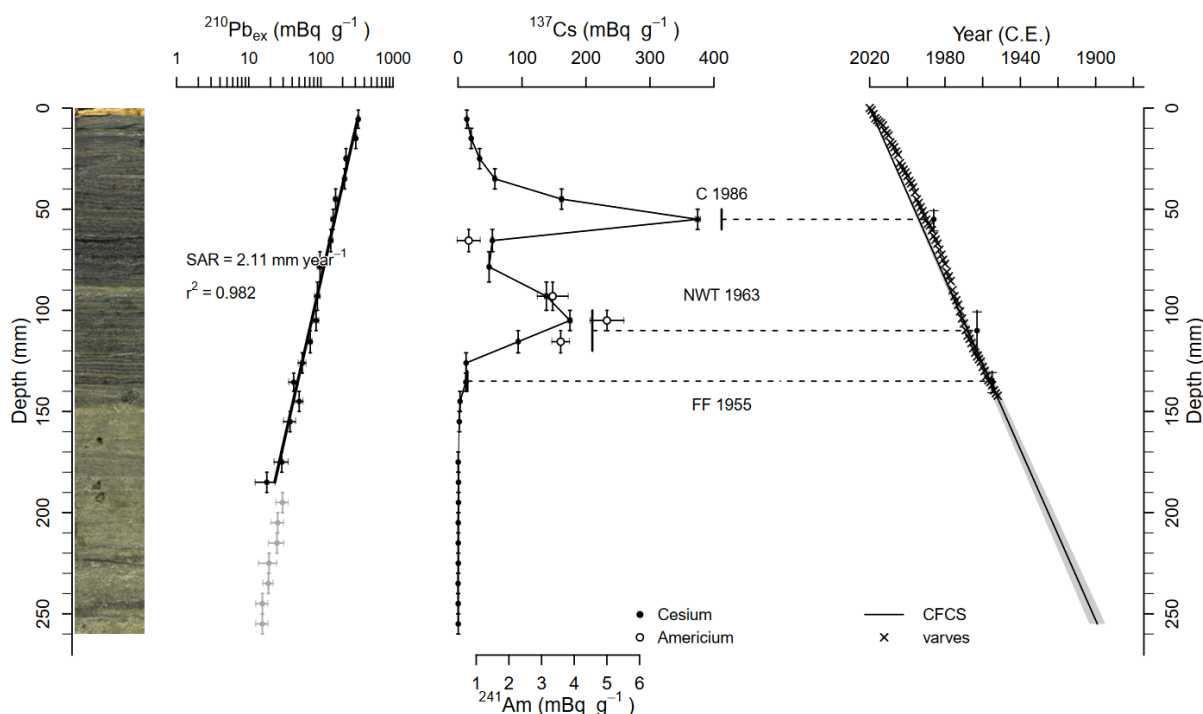
281
282   **Fig. 7: Age-depth model based on short-lived radionuclides for the top of the AIG20-01 sequence. The model is derived from**
283   **the serac package. From left to right: picture of AIG20-01 sediment; ^{210}Pbex; ^{137}Cs and ^{241}Am activities with the CFCS age**
284   **model. In the age-depth model, the crosses correspond to lamina counting.**

285   Based on sediment core visual observations and photos, clear laminae were counted from the top of the sequence (AIG20-

286   01) to 16 cm (MCD). Each clear lamina was considered a year of sediment deposition (Ca-rich clear laminations are

287   associated in other French alpine lakes with late spring to summer seasonal biogenic deposition (Giguet-Covex et al.,

288   2010). Ages resulting from lamina counting are in good agreement with the radioelement age-depth model (Fig. 7). In

289   sediment sequences from the Lake Aiguebelette deep basin, laminations can be considered as varves (Fig. 3, Fig. 7).

290   Unfortunately, varved sediment is not continuous or present in the whole sequence. Varves can only be counted on the

291   uppermost part of the deep basin sequences.

292

4.4.2 Palaeomagnetism: characteristic remanent magnetization (ChRM) versus depth

293

294 In most analyses of NRM demagnetization, using orthogonal diagrams (Zijderveld, 1967), a clear magnetic component

295 aligned with the origin is observable. Therefore, the calculated ChRM directions of the stable magnetic component is

296 confidently interpreted as parallel to the Earth magnetic field. The ChRM versus depth results are compared to the existing

297 geomagnetic field models as explained in Crouzet et al., 2019a (SM4). Data from each sediment core section are corrected

298 to have the same declination orientation (towards the north). Inconsistent measurement points at the top and base of the

299 sections were removed. The correlations of the ChRM data with the continuous global geomagnetic field model Cals10K

300 (Korte et al., 2011) add a total of 18 time–depth constraints (SM4 and Fig. 8). This new age-depth model for Lake

301 Aiguebelette deep basin sequence AIG17III is more robust (with additional data) than the previous age-depth model

302 available in Banjan et al. (2023).

Can you mention here which timeframe this covers?

Natural Hazards
and Earth System
Sciences
Discussions
Open Access
EGU

Varve counts ??
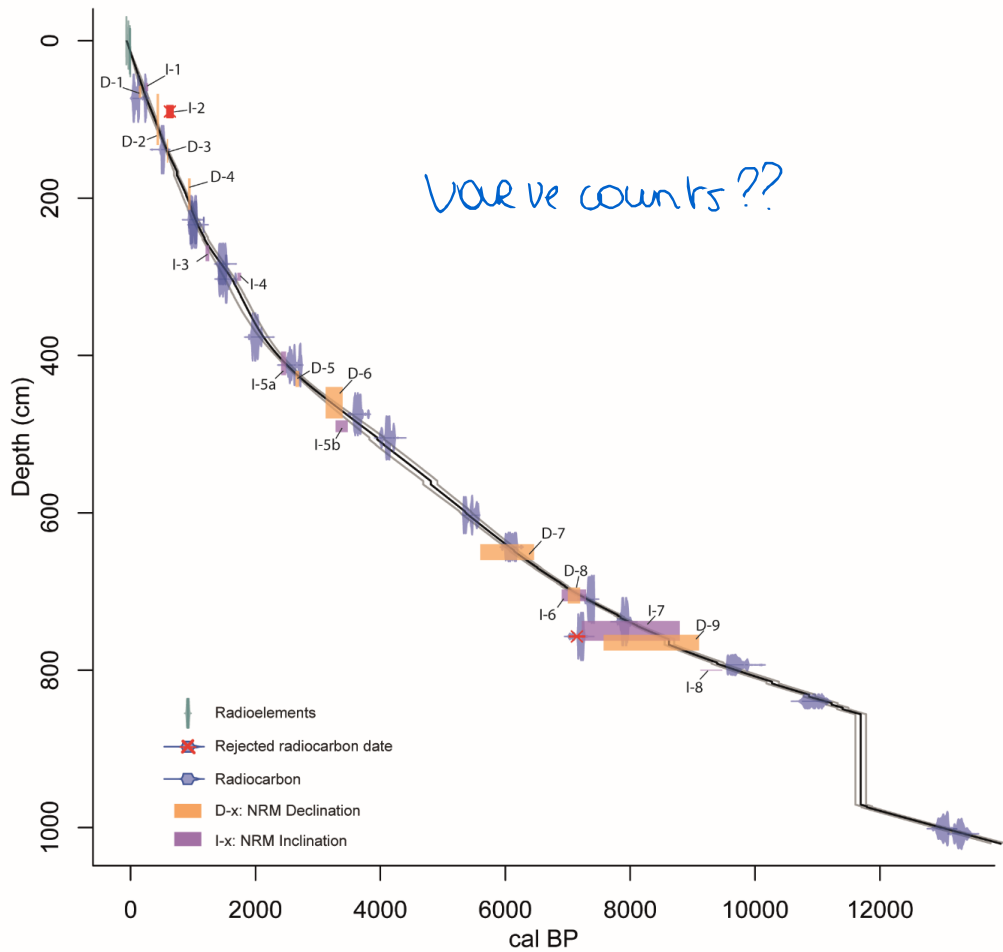
Fig. 8: Age-depth model for core AIG17III combining radioelement data (green), ^{14}C ages (dark blue) and magnetic features based on declination (orange) and inclination (purple) data. The vertical bars correspond to the depths and ages of the event layers in the sediment sequence.

?

4.4.3 Age depth model construction

The long sequence's age-depth model gives robust chronological estimations of sediment deposition. To better constrain the age of the most recent event layers, varve counting on the upper 16 cm and correlation with core AIG20-01 on which short-lived radioelement dating was performed. Correlations between the different cores used to constrain the chronology

is available

312   of the event layers are available in SM-2 and SM-5. The nineteen previously published radiocarbon ages (Banjan et al.,

313   2023) were calibrated with the Intcal20 calibration curve (Reimer et al., 2020).

314

315   The eighteen palaeomagnetic time–depth constraints and the nineteen radiocarbon ages on terrestrial vegetal

316   macroremains previously published allow us to constrain the depositional timing of AIG17III sediments through the entire

317   Holocene period (see Table 2). Prior to modelling the age-depth relationship of the sediment sequence, an event-free

318   master core was built (Sabatier et al., 2022). Then, the age-depth model, including all the available data, was created with

319   the R package clam smooth spline function (Blaauw 2010). The first 10 meters of the sequence cover the last 13000 yr

320   cal BP (Fig. 8). Therefore, a Holocene event layer chronology can be built with good accuracy on the basis of this robust

321   multiproxy age-depth model.

322   **5 Discussion**

323   **5.1 Palaeoseismological interpretation of event layers**

324

325   A total of 55 event layers deposited during the Holocene have been identified. Thirty-two event layers have a thickness

326   ⩾ 0.5 cm, and 23 have a thickness < 0.5 cm. Event layers deposited during the Late glacial period are not mentioned in

327   this discussion for two main reasons: 1) the age-depth model is not well constrained for the entire Holocene; 2)

328   sedimentation and triggering processes of the event layer deposition may have been different during the Late glacial than

329   during the Holocene.

330   In cores AIG16-06 and AIG16-05, retrieved from the eastern side of the deep basin, several event layers were identified,

331   and in the first 150 cm of the sequences none of them were found to be synchronous with events of the AIG17III core

332   (SM-1). The higher number of event layers identified in the AIG16-05 and AIG16-06 cores is certainly related to the

333   presence of steep slopes on the eastern side of the deep basin, making the coring location of these two sediment sequences

334   more prone to archive event layer deposits than the AIG17III.

335

336   As suggested in several studies (Chapron et al., 1999; Carrillo et al., 2008; Beck, 2009; Campos et al., 2013; Crouzet et

337   al., 2019 b), seismically induced homogenites should be characterized by specific magnetic fabric and grain size

338   characteristics. In parallel, several studies have shown that the AMS foliation is higher in Hm than in continuous

339   sedimentation, interpreted as due to the oscillation of the water mass during a seiche induced by an earthquake (Petersen

340   et al., 2014; Rapuc et al., 2018; Yakuppoglu et al., 2022). The geochemical signature of these event deposits allows us to

[handwritten note: ⌐> What about the higher Ti content?]

341   identify that the sedimentary material was previously deposited on the slope of the lake and then remobilized (Fig. 4). In

342   this study, event layers were identified with the same criteria (multiproxy data: XRF logarithmic geochemical ratios, D50

343   and D90 grain-size data, high AMS foliation values, low IRM amplitudes (Fig. 4)) as the thickest event layer of the deep

344   basin sequence, deposited at the Younger Dryas - Early Holocene transition (Banjan et al., 2023). Based on the

345   interpretations of grain-size, geochemical data associated with high AMS foliation and low IRM amplitudes, we suggest

346   that Hm and Tu+Hm event layers with a thickness > 2 cm are of seismic origin, with a good confidence level. A total of

347   eight event layers have a thickness > 2cm. *[handwritten note: ⟶ This refers to the long core?]*

348   For event layers between 2 cm and 0.5 cm thick (24 of them are identified), the grain size pattern in the Passega diagram

349   (D50 and D90, Passega, 1964, Sabatier et al., 2022), shows a similar trend with those interpreted as originating from

350   seismically induced process (ie > 2 cm and showing high AMS foliation). Such a similar trend suggests that their seismic

351   origin is plausible (Sabatier et al., 2022), however with a moderate confidence level.

352   The 23 event layers with a thickness < 0.5 cm, cannot be interpreted as seismically induced with a great confidence (there

353   is less data available due to the measurements step being of approx 0.5 cm or the need of a sample with a minimal

354   thickness greater than 0.5 cm). For this reason, there is a specific distinction in the following discussion between event

355   layers thicker than 0.5 cm and those thinner than 0.5 cm (Fig. 9).
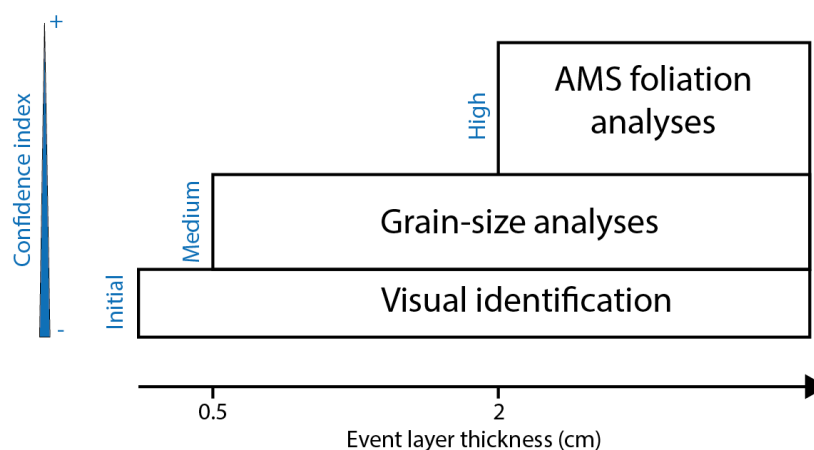
356

357   **Fig. 9: Qualitative chart showing the confidence index for the identification of seismically-induced event layers based on their**
358   **thicknesses. Geochemical and IRM analyses support the interpretations for deposits ⩾ 0.5 cm.**

359

5.2 Correlations between the event layers and the seismic catalog

5.2.1 Earthquake Sensitivity Threshold Index (ESTI) method

360

361

362 A synthesis of all the event layers from cores AIG16-05, AIG16-06 and AIG 17III was made to correlate them to the

363 events from the seismic catalogs (SisFrance and FCAT-17). The deposition time of these event layers is constrained by

364 core-to-core correlations based on observations, IRM data and age-depth model of the AIG17III sequence (Fig. 6).

365 In the top 200 cm of the AIG16-05 sediment sequence, seven event layers are observed and their depositional times

366 (between 945 and 1824 CE) correspond to the period covered by the SisFrance historical seismic catalog at the French

367 national scale (Jomard et al., 2021).

368 Four consecutive event layers deposited between 1921 and 1929 CE are however not included in this count. There is no

369 record of a local to regional earthquake occurring at that time, as well as no record of significant flooding events. On the

370 other hand, the exploitation of the lake (for tourism and industrial activities (i.e., energy production)), led to numerous

371 developments within the lake and in its periphery starting from the end of the 19th century. Dredging activities in the lake

372 are noted in the archives at a period compatible with the event layer deposits. In consequence, for the sake of this study,

373 these four event layers are not considered.

374 *↳ but you did previously consider them as seismically triggered?*

375 In the SisFrance catalog, several earthquakes occurred in the same time range as the deposition of each of the AIG16-05

376 event layers. To test the possible association between these earthquakes and the event layers, we first applied the method

377 developed by Wilhelm et al. (2016), based on the determination of the sensitivity of a lake to record seismic deposits.

378 We plotted the conceptual diagram "epicentral distance to the lake versus epicentral MSK intensity" (Fig. 10) based on

379 data contained in the SisFrance catalog (Jomard et al., 2021) and then added the earthquake sensitivity threshold index

380 (ESTI) developed by Wilhelm et al. (2016). The ESTI empirical limit is supposed to separate the recorded from the

381 nonrecorded earthquakes in the lake. It represents the sensitivity threshold for a lake to record seismic events and is

382 defined by the equation $y = a.\ln(x) + b$, where x is the distance between the lake and the epicenter and y is the epicentral

383 intensity of the historical earthquake. It is applied to Lake Aiguebelette using the same slope as defined in Wilhelm et al.

384 (2016) for the same area (Western Alps), with $a = 1.13$ (Fig. 10 (B)). Using such a threshold line implies that the effects

385 of the regional geology may be considered negligible and homogeneous across the studied area.

386

387 The mean sedimentation rate in Lake Aiguebelette covering the first 1.7 m of sediments (≈ past 700 years CE) is 2.1

388 mm.yr^{-1}, which is close to the sedimentation rate of the Central French Alps Lake Laffrey (Nomade et al., 2005; Wilhelm

389 et al., 2016). According to previous studies, Lake Laffrey (ESTI value between 0.18 and 0.19) has a relatively high

↳ please elaborate on what this means

390   sensitivity to seismic events compared to other lakes in the French Alps and beyond (Wilhelm et al., 2016; Rapuc et al.,

391   2018). The ESTI value was attributed to Lake Aiguebelette taking into account the 2.1 mm.yr^{-1} sedimentation rate value

392   and the position of the other alpine lakes in the 'EST Index vs. sedimentation rate' chart (Fig. 10 (A)). In this chart, a

393   third-degree polynomial fit was used (equation: $0.004969x^3 - 0.0364 x^2 + 0.09273x + 0.1028$) and for $x = 2.1$ mm.yr^{-1}, an

394   ESTI value of y= 0.183 was obtained for Lake Aiguebelette. Hence, in Fig. 10 (B), the inverse value of the estimated

395   ESTI (≈ 5.55) is used as the intercept of the threshold line with the intensity axis at an epicentral distance of 10 km.
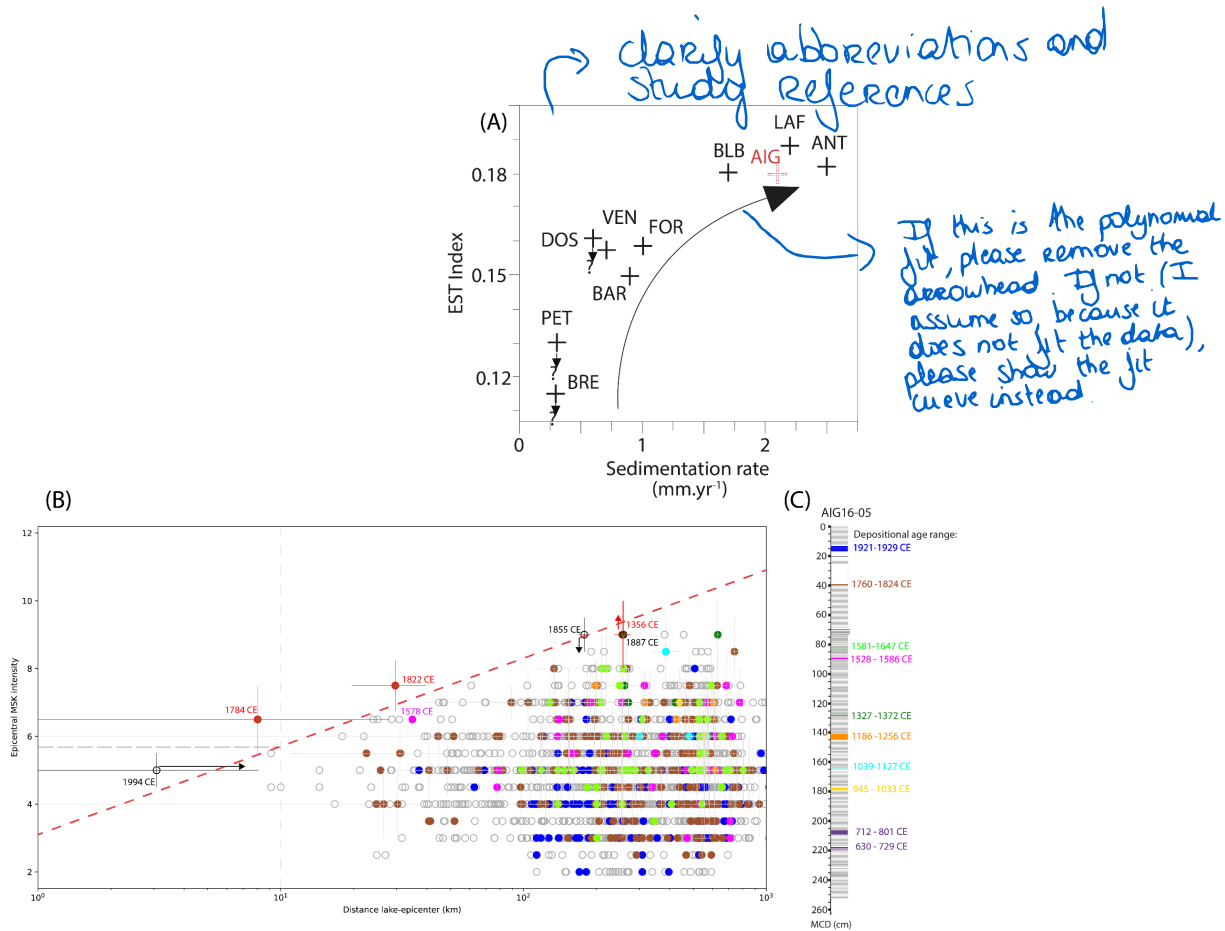
396
397   **Fig. 10: (A) ESTI plotted against the sedimentation rate for several French alpine lakes (black crosses) and Lake Aiguebelette**
398   **(red cross), (modified from Wilhelm et al., (2016)); (B) Epicentral distance to the lake vs. epicentral MSK intensity diagram for**
399   **historical earthquakes contained in the SisFrance catalog (dots), with their associated uncertainties (Jomard et al., 2021). The**
400   **sensitivity threshold is represented by a red dashed line. Historical earthquakes that occurred at the time of deposition of a**
401   **specific event layer are colored in the same way. Transparent dots correspond to earthquakes that occurred at a time not**
402   **compatible with the event layer deposition. Red/black contoured dots and arrows are historical earthquakes specifically**
403   **discussed in the main text. (C) AIG16-05 sediment sequence with the identified event layers.**

404 Once the threshold line is fixed, we can observe that some seismic events from the SisFrance database have an absolute

405 position above it but are not compatible with the depositional time of the archived event layers (e.g., the 1994 CE event,

406 which is the closest to Lake Aiguebelette in this diagram, or the 1855 CE event) and that events that may be situated

that is the same as before? You mean 'below are'?

407 above are not (e.g. the 1356 Basel earthquake). A possible way to discuss these apparent discrepancies is to integrate

408 uncertainties contained within the SisFrance database in the diagram (Fig. 10 (B)). Indeed, each earthquake in the

409 SisFrance database is associated with a number of uncertainties, depending on the knowledge we have on each event

410 (Scotti et al., 2004; Jomard et al., 2021). By considering uncertainties associated with epicentral earthquake parameters

above

411 (intensity and location), all these events could be either placed over or below the ESTI line (Fig. 10 (B)).

412 Both the 1784 and 1822 CE earthquakes have an absolute position well above the sensitivity threshold, and both seismic

413 events are compatible with the depositional time range of the same event layer (between 1760 and 1824 yr cal CE). At

? only if the risk at the lake is higher, but this you did not discuss

414 first glance, it would seem more probable if the triggering event was the 1822 CE Bugey earthquake event because it was

415 the strongest known local seismic event, also formerly identified within the sediments of Lake Le Bourget (Chapron et

416 al., 1999). However, the ESTI approach here is not capable of differentiating which earthquake is archived in Lake

417 Aiguebelette, even in considering their associated uncertainties.

418 In the conceptual diagram based on Wilhelm et al. (2016), it seems mandatory to consider the uncertainties associated

419 with historical earthquakes. However, because these uncertainties are mainly based on written archives and hence rather

420 qualitative in nature, especially concerning the epicentral characteristics (Jomard et al., 2021), the epicentral intensity

421 might not be the best parameter to discriminate which of the two seismic events might have triggered event layer

422 deposition in the lake. More generally, this method alone might not be sufficient to identify the seismic events to which

423 a lake may be sensitive. In the following section, ground motion prediction equations (GMPE) will be used to complement

424 and discuss results from the ESTI approach. Apart from uncertainties associated with historical earthquakes, another

425 important aspect to consider is the incompleteness of historical seismic catalogs. For instance, it is probable that the event

426 layer deposited in the Lake Aiguebelette deep basin between 1327 and 1372 yr cal CE cannot be related to the 1356 CE

427 Basel earthquake itself but to an earthquake that occurred closer to the lake (local event), not recorded in the historical

428 catalogs, which are incomplete at that time.

→ Approach similar to Daxer et al. (2024)

429 **5.2.2 Contribution of ground motion prediction equations (GMPE)**

430 Ground motion parameters and models can be useful to target the events to which a given lake is sensitive (Strasser et al.,

431 2013; Avşar et al., 2016; Moernaut, 2020). In Lake Aiguebelette, the GMPE approach was first used to better discriminate

432 which of the 1784 or 1822 CE seismic events might have produced the strongest ground motions at the lake. Then, the

433 approach was extended to the overall historical earthquake catalog using the FCAT-17 seismic catalog (Manchuel et al.,

434   2018) which provides magnitude-depth estimates for historical earthquakes contained in the SisFrance database. For some

435   strong and distant events located far from the French boundary (>20 km), the EPICA catalog is used to complement the

436   FCAT catalog (Rovida et al., 2022). In this light, PSA values were calculated with GMPE after Bindi et al. (2017) and

437   Akkar et al. (2014) for all seismic events of the FCAT-17 catalog. These GMPEs were selected because the metrics used

438   (hypocentral distance) as well as their validity domain are compatible with our dataset. Pseudoseptral acceleration (PSA)

439   values were calculated and plotted in Fig. 11 for two frequencies representative of a low frequency content (0.5 Hz) and

440   a high frequency content (5 Hz). Because many parameters related to the source of the earthquakes, the path of the seismic

441   waves and the geological parameters of the site can contribute to modifying the seismic motion, we focus in the first

442   approach on the relative differences between earthquakes of interest rather than on the absolute values of ground motion.

443
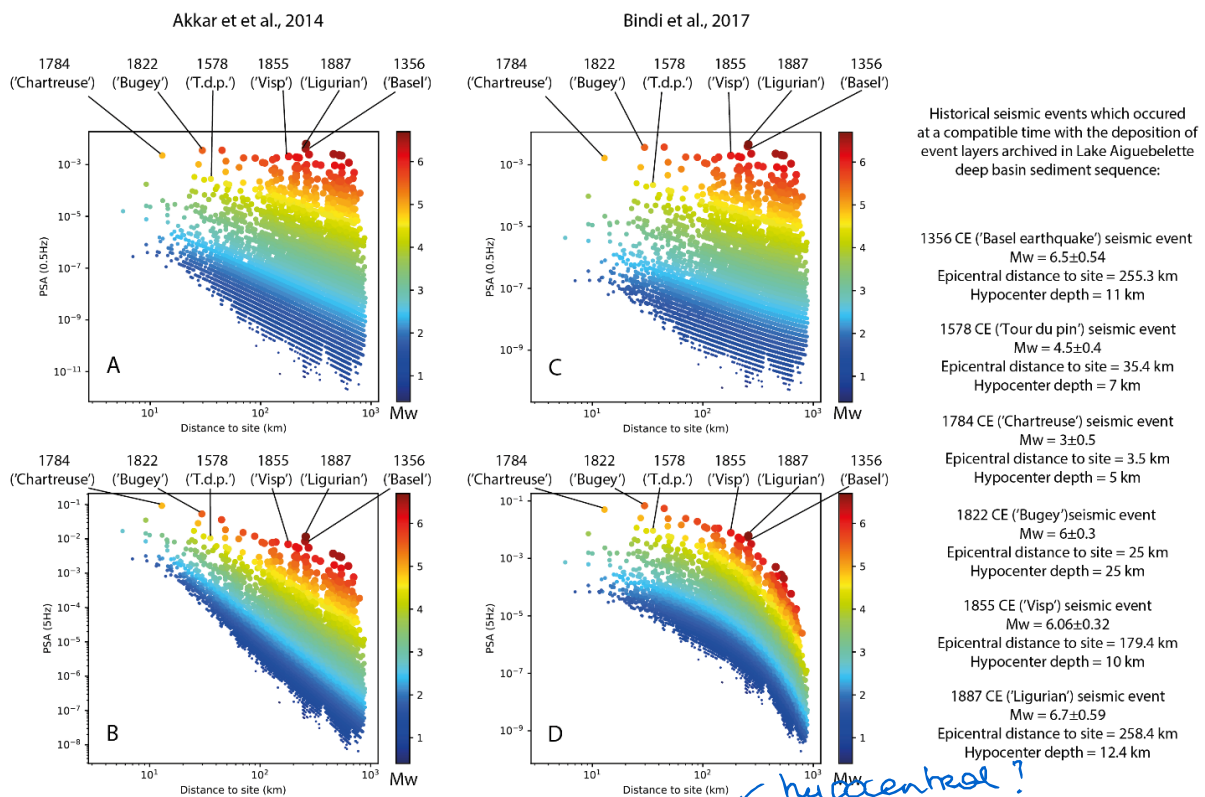
444
445   **Fig. 11: Calculated PSA values for several seismic events versus their epicentral distance to Lake Aiguebelette. PSA values are**
446   **calculated with the GMPE from Akkar et al., 2014 (A, B) and Bindi et al., 2017 (C, D). A and C are plotted for a 0.5 Hz input,**
447   **B and D for a 5 Hz input. Dots correspond to all events from the FCAT-17 earthquake catalog. Events discussed in the main**
448   **text are reported as 1356 ("Basel"), 1578 ("Tour du pin"/ "T.d.p."), 1784 ("Chartreuse"), 1855 ("Visp"), and 1887 ("Ligurian").**
449   **Uncertainties in the PSA values are not displayed, in this case, the relative PSA value for each event is compared to the others.**

24

450   The results of this seismic motion-oriented approach do not give a strong argument to discriminate which of the 1784 CE

451   or 1822 CE earthquakes led to the deposition of an event layer in Lake Aiguebelette. Indeed, the expected ground motions

452   for the two events are ~~globally~~ *overall* very close. Only Akkar's law for a frequency of 5 Hz shows a significant difference

453   between the two events, with a higher ground motion associated with the 1784 CE earthquake.

454   By considering the whole catalog, it is possible to highlight a general tendency, particularly concerning the relative

455   sensitivity of the lake to local events or to those more distant. For a low-frequency input (0.5 Hz, Fig. 11 (A) and (C)),

456   many distant events have PSA values of the same order as those associated with the 1784 CE and 1822 CE earthquakes.

457   If the lake is sensitive to this frequency content, then it is likely that a greater number of events would have been recorded.

458   For instance, the events of 1356 CE, 1855 CE and 1887 CE, of comparable magnitude and distance, would present the

459   highest spectral accelerations.

[handwritten margin note: → the possible incompleteness of a catalog is not really a solid argument. Why would it not be recorded? It is due to the threshold]

460   While the presence of the Basel earthquake in the sediments of Lake Aiguebelette is debatable (although unlikely in our

461   opinion, cf. discussion in the previous section), the 1887 CE event is clearly absent. A similar observation can be made

462   regarding the Visp earthquake (1855 CE), which would potentially be recorded in the ESTI approach and should also be

463   recorded if the lake was sensitive to low-frequency content. However, no event-layer corresponds to this event.

464   Conversely, for a higher frequency input (5 Hz), strong and distant seismic events from Lake Aiguebelette present

[handwritten note: → Of course they do, because high f is attenuated faster ...]

465   significantly lower PSA values compared to moderate and nearby events, which is more in line with the fact that few

[handwritten note: → BUT lakes are sensitive to low-f content !! see Van Daele et al (2019)]

466   events are archived in lake sediments. In this case, the event layers archived in the Lake Aiguebelette deep basin sediments

467   would be representative of a local to regional seismic chronicle.

468   In this light the event layers that were deposited during the historical period (Fig. 6) covered by the SisFrance database

469   could be interpreted as follows:

470   1760-1824 yr cal CE: This event layer corresponds to either the 1784 or the 1822 earthquakes. Based on the GMPE

471   method, if Lake Aiguebelette has a higher sensitivity to high frequencies, the 1784 CE event can be favoured as the

472   triggering process for this event layer (Fig. 11 (B), SM-4, SM-6). From a sedimentological perspective, it might be

473   possible to favour one of the two seismic events as a trigger for the deposition of this event layer. Based on the SEM

474   analyses of the lamina at the top and bottom of the event layer, it is possible to constrain the season during which the

475   event layer was deposited (Fig. 3 B). The lamina that was deposited before the event layer is Ca-rich and can be interpreted

476   as a summer varve. ~~Additionally, the lamina that was deposited before the event layer is Ca-rich and can be interpreted~~

477   ~~as a summer varve.~~ Additionally, the lamina topping this event layer is Al-rich and can be interpreted as a winter varve

478   (Fig. 3 B; Giguet-Covex et al., 2020). It is therefore possible to suggest that the event layer was deposited between summer

479   and winter. It is known that the 1784 CE seismic event occurred on the 15th of October

480   (https://www.sisfrance.net/seismes/details/380016), while the 1822 CE seismic event occurred on the 19th of February

Natural Hazards
and Earth System
Sciences
Open Access
EGU
Discussions

481 (https://www.sisfrance.net/seismes/details/10007). On this basis, it is possible to favor the 1784 CE seismic event as a

482 possible trigger to event layer deposition in the Lake Aiguebelette deep basin. It also confirms that this lake is more

483 sensitive to high frequencies of the PSA content. This means that the ground motions of this seismic event were close to

484 the sensitivity threshold of Lake Aiguebelette;

485 1581-1647 and 1528-1586 yr cal CE: Only one regional historical earthquake corresponds to these event layers, occurring

486 on the 20th of May 1578 (Io = VI-VII in SisFrance). This event is very poorly characterized (location and intensity are

487 arbitrarily defined in SisFrance). However, the knowledge concerning historical earthquakes in the region is poor before

488 the XVIIIth century (Table 2). This means that some events, even relatively strong ones such as the one reported in 1578

489 CE may be missing in the catalog;

490 1327-1372 yr cal CE: The situation is even worse for the XIVth century. As discussed before, even if the major Basel

491 earthquake could correspond in date with the event layer, it is highly probable that a local moderate earthquake will not

492 appear in the SisFrance database;

493 1186-1256 yr cal CE: Same as previous. However, a question may arise regarding the relationship between this event

494 layer and the Mount Granier collapse (Berlioz, 1987; Nicoud et al., 1999), which occurred in 1248 CE and constitutes the

495 most important and local natural hazard event reported in medieval times. Although it is not possible to demonstrate the

496 existence of a potential triggering earthquake for this collapse, the question deserves to be explored in the future.

497

Century	XIV th	XV th	XVI th	XVII th	XVIII th	XIX th	XX th
Nb of Earthquakes	0	0	1	0	11	28	40

498

499 **Table 2: Total number of earthquakes per century reported in the SisFrance database (Jomard et al., 2021) within a 50 km**
500 **radius around Lake Aiguebelette.**

501 The approach presented in this study is complementary to the work developed by Wilhelm et al. (2016), as it completes

502 the discussion for establishing an event layer chronicle. However, it should be noted that the approach developed in this

503 paper is relatively preliminary as it does not, for example, consider local conditions that could lead to changes in seismic

504 motion for certain frequency ranges (Ergin et al, 2004; Maufroy et al, 2015, Courboulex et al., 2020) and thus could alter

505 the proposed interpretations.

5.3 Towards a local seismic chronicle?

In Lake Aiguebelette, we considered event layers to be seismically-induced with a confidence level depending on their thickness (Fig. 9). In addition, we propose that these events were mainly triggered by local earthquakes. In the following, we will discuss the extent to which the data acquired can or cannot be used to construct a local seismicity chronicle.

First and foremost, it is important to remember that no clear relationship was reported in the literature linking the thickness *[handwritten: → there are several studies in Chilean lakes doing this …]* of the event layer and the severity of the ground shaking. However, for Lake Aiguebelette, it is interesting to report that a return period of ≈3000 to 4000 years (±500 years, based on the age-depth model uncertainties) is visible for the thickest event layers (thickness ≥ 4.5 cm) in Fig. 12A. This return period is comparable to that estimated from seismological data *[handwritten: please elaborate]* by Banjan et al., (2023) concerning seismic events occurring within a 10 km radius around the lake, equal to ≈3500 years for a M5 earthquake and ≈5000 years for a M ≥ 5.5. Beyond what may be the most important local seismic events, we hereafter explore two hypotheses to discuss a seismic chronicle covering the Holocene: 1- considering all the identified event layers as being seismically induced, and 2- taking into account only the ≥ 0.5 cm thick event layers, for which greater confidence can be placed in their seismic origin. The occurrence of event layers over time is depicted in figure 12. Associated to the thickness, the frequency (101-years running sum), the interval of time between each deposit *[handwritten: all]* and the sedimentation rate are together analysed. The latter is considered to have a strong influence on lake sensitivity to earthquake shaking (Wilhelm et al., 2016; Sabatier et al., 2022) *[handwritten: ↳ but not if you consider surficial remobilisation]*

From this dataset, it is possible to identify 3 main stages (Fig. 12; Table 3) as follows.

1) The first stage corresponds to the period ranging from -9890 to -2000 yr cal CE during which a frequency of 4.56 event layers/kyr (independently of their thicknesses) is observed. Considering only event layers ≥ 0,5cm, the frequency is equal to 2.66 event layers/kyr. The mean sedimentation rate during this period of time is low, equal to ~0.04 cm/yr.

2) In the event layers chronicle, a period of quiescence is visible between -2000 and 0 yr cal CE (Fig. 12; 13), where no event layer ≥ 0.5 cm is archived in the lake. The sedimentation rate increases up to a mean value of 0.12 cm/yr.

3) Since ~ 0 yr cal CE, the sedimentation rate in the Lake Aiguebelette deep basin continues to increase, highlighting more significant short-term variations (mean rate of 0.22 cm/yr). This trend goes along with the highest observed frequency of event layers deposition, 7.45 event layers/kyr in total and 5.45 event layers/kyr for event layers≥0.5 cm (Figs. 13 and 14, Tables 2 and 3).
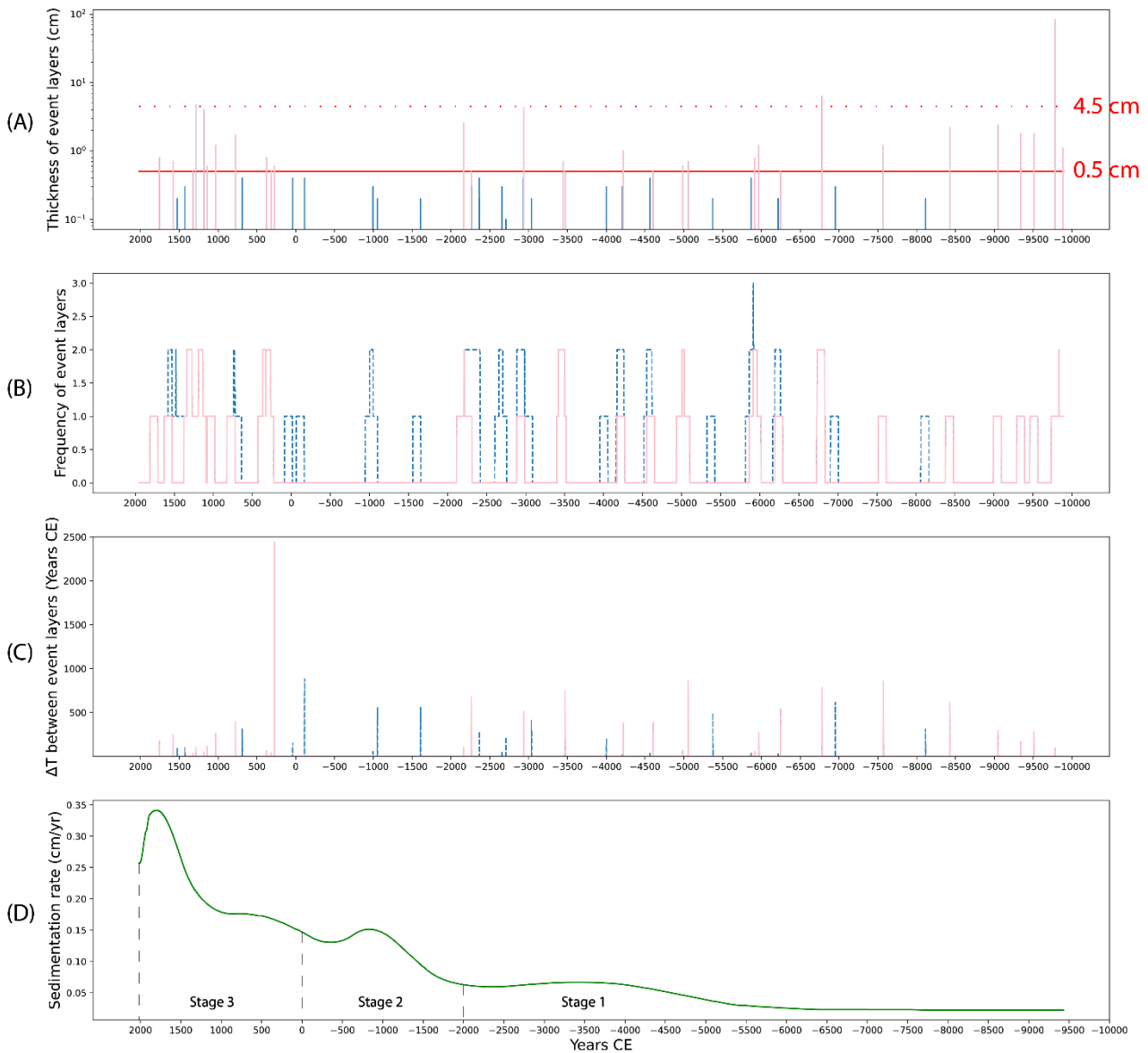
Fig. 12: Different parameters characterizing the event layers deposited in the deep basin sequences of Lake Aiguebelette, are represented over the last 11800 yr cal BP (since -9890 yr cal CE). (A) thickness, (B) frequency (101-year running sum), (C) interval of time between each deposit, (D) sedimentation rate. The red horizontal line on the upper chart (A), represents the limit between event layers with a thickness ⩾ 0.5 cm, which are represented in light pink. The other event layers are represented in blue. The red dotted line represents the limit for a thickness of 4.5 cm. It is possible to see a time interval of the same order between the event layers with a thickness ⩾ 4.5 cm. The black dotted lines on the bottom chart indicate three separate periods of time: stage 1, from -9890 to -2000 CE; stage 2, from -2000 to 0 CE and stage 3, from 0 to 2017 CE.

[Handwritten annotation: Exactly. Why don't you make this comparison only for the long core site, so that you can rule out changes in sensitivity just dependent on the coring site?]

541 A comparison between the interpreted stages 1 and 3 highlights a clear relationship between the increase of the

542 sedimentation rate through time and the increasing frequency of event layers archived in the lake. It should be noted,

543 however, that a rather limited ~~part of~~ the number of event layers recorded during stage 3 *[handwritten: 1 ?]* may be due to the greater number

544 of event layers found in core 16-05 in comparison to core 17-III (see section 5.1, Table 3). For instance, such an increase

545 in seismically induced deposits has been described in Lake Bohinj (Rapuc et al., 2018) and Lake Iznik (Gastineau et al.,

546 2021) or other lakes in the Alps (Wilhelm et al. 2016) in relation to increased erosion related to human activities and thus

547 could produce misinterpretation in order to build a seismic chronicle. Hence, the higher frequency of earthquake related

548 event-layers observed in Lake Aiguebelette over the last 2000 years can be interpreted as related to an increasing

549 sedimentation rate enhancing the sensitivity of the lake sediments to earthquake shaking, rather than to an increased

550 number of earthquake (i.e. enhanced seismicity rate).

551 However, this observation is no longer valid for stage 2, during which no event layer was observed despite the increased

552 sedimentation rate. The absence of thick event layer during stage 2 could tentatively be explained by a lower water level,

553 as proposed in other lakes worldwide (Osleger et al., 2009; Zhang et al. 2014). This hypothesis is based on the observation

554 of pile-dwelling sites (palafittes) in Lake Aiguebelette correlated to low-water level, sociological and climatic changes

555 (Pétrequin and Bailley, 2004). Dendrochronological studies show 3 main occupation phases during the late Bronze-Age,

556 at approximately -1100 CE; -1000/-990 CE and from -930 to -805 CE (Billaud and Lachenal, 2017). However, the

557 influence of rather limited lake level variations (few meters in the case of Lake Aiguebelette) on lake sediment stability

558 under seismic loading is unknown and most probably limited considering the depth of the drilled lake basin (~70m depth).

559 Variations in conditions outside the lake are therefore more likely to explain the absence (or quasi-absence) of event layer

560 during stage 2. In this case, variations in climate and/or seismic activity would be the most likely explanations.

561 Considering the climatic conditions during stage 2, available data in the Alps seem to show a greater frequency of floods

562 over the period corresponding to stage 2, as is the case for Lake Iseo (Rapuc et al., 2019) and other lakes of the southern

563 central Alps (Wirth et al., 2013), for example, where an increase in the number of floods and related erosion is observed

564 over the period 2200-4200 yr cal BP. The peak of sedimentation rate recorded in Lake Aiguebelette during this period

565 (Fig. 12 D) is consistent with these observations. On the other hand, the absence of event layers clearly shows that this

566 part of the lake is not sensitive to record flooding events, and push towards the possibility to consider the event layer

567 record as a seismic chronicle. We therefore interpret our observations as being more likely linked to a seismic quiescence

568 for this specific period.

569 *[Handwritten annotation: → How does this relate to other Alpine EQ studies?]*

570

Natural Hazards
and Earth System
Sciences
Discussions

Stage	1	2	3
Time interval	-9890 to -2000 yr CE	-2000 to 0 yr CE	0 to 2017 yr CE
Mean sedimentation rate (cm/yr)	0.04	0.12	0.22
Number of all event layers archived in the deep basin sediment sequences	36 event layers 4.56 event layers/ kyr	4 event layers 2 event layers/ kyr	15 event layers* 7.45 event layers/ kyr (*including 4 events only present in the AIG16-05 sequence).
Number of event layers with a thickness ≥ 0.5 cm archived in the deep basin sediment sequences	21 event layers 2.66 event layers/ kyr	0 event layers 0 event layers/ kyr	11 event layers* 5.45 event layers/ kyr (*including 3 events only present in the AIG16-05 sequence).

Table 3: Number of event layers deposited in the deep basin based on the sum of all the event layers archived during two different time intervals.

The above discussion suggests that the lake's sediment event layers likely result from past seismic activity and that the event layers archived in the lake are probably representative of a local seismic chronicle. However, this chronicle is possibly incomplete (depending on the location of the coring) and not homogeneous over time depending on temporal variation of both lake parameters (i.e. sedimentation rates) and external forcing (i.e. seismicity rates). To deepen our understanding, we performed a statistical analysis based on the events archived in the lake during (A) stage 1 (from -9890 to -2000 yr cal CE), where low variations in the sedimentation rate are observed and could explain the origin of the triggering events, and (B) during stage 3 (from 0 to to 2017 yr cal CE) where high temporal variations in the sedimentation rate most probably preclude this kind of approach.

Williams et al. (2019) show that non-random failure seems to be the norm for faults in the seismogenic crust, with 58% of the studied chronologies supporting this interpretation. Their study is based on a compilation of 31 published

584   earthquake chronologies (each chronology includes at least 5 dated earthquake events; the analysed chronologies include

585   strike-slip, normal, and reverse faults in both plate-boundary and intraplate environments). Model distributions for several

586   laws (lognormal, gamma, Weibull and exponential) may be representative of a specific type of seismicity. The recurrence

587   time of strong earthquakes usually follows a Weibull distribution with exponent $\alpha_1 < 1$ (Nishenko and Buland, 1987;

588   Hasumi et al., 2018; Moernaut et al., 2018; Praet et al., 2020). The exponential distribution is the simplest law and can

589   trivially suggest that earthquakes are independent and occur randomly. The lognormal law is often used empirically, as

590   most of the time it fits the data well, suggesting that the earthquake occurrences are quasi-cyclical (Matthews et al. 2002;

591   Zöller et al., 2008; Zöller, 2018). A gamma distribution is generally associated with the interoccurrence times (e.g., Corral,

592   2004). They correspond to the intervals between consecutive earthquakes on all faults in a region; this is distinct from

593   recurrence times, which are the time intervals between large (characteristic) earthquakes on a single fault or fault segment

594   (Abaimov et al., 2008).

595
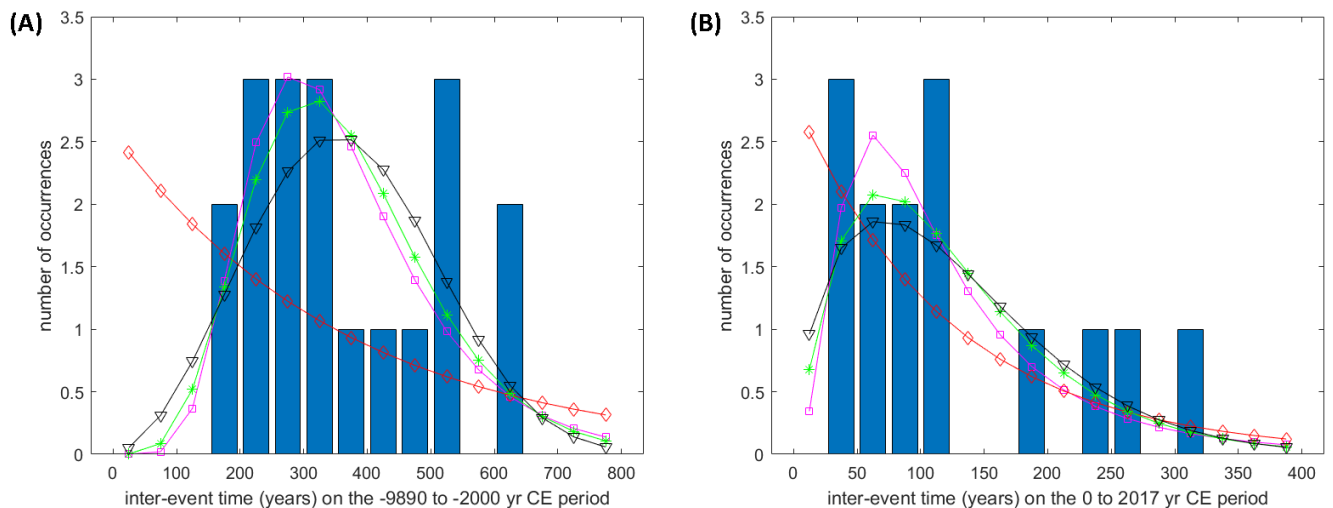
596

597   **Fig. 13: Number of event layers deposited in Lake Aiguebelette deep basin vs. the time gap between the deposition of each event**
598   **layer ≥ 0.5 cm. Model distributions are presented for Lognormal (in magenta), Gamma (in green), Weibull (in black) and**
599   **Exponential (in red) distributions best fitting the data. (A) Over the -9890 to -2000 yr cal CE period of time. The fit values for**
600   **each distribution are respectively of: 45.77 (lognormal), 45.85 (gamma), 46.31 (weibull) and 56.72 (exponential). (B) Over the**
601   **0 to 2017 yr cal CE period. The fit values for each distribution are respectively: 34.12 (lognormal), 34.45 (gamma), 34.75**
602   **(weibull) and 36.51 (exponential).**

603   In the histograms (Fig. 13), the event layers (Hm and Tu+Hm) with a thickness ≥ 0.5 cm are represented, in order to

604   conserve a robust interpretation. The fit values for each distribution are calculated by minimizing a cost function based

605   on Poisson statistics. The relative comparison of these fit values (Fig. 13) does not suggest that a specific distribution

606   provides a better fit than the others. For the event layers ≥ 0.5 cm, the histograms (Fig.13) over the 2 periods show

607   (visually) compatibility with several distributions (lognormal, gamma and Weibull). Only the exponential distribution

608   (i.e. random occurrences) can be rejected with confidence. The fit values (Fig.13) should be interpreted relatively to one

609   another. Hence, except for the exponential model, the three other models have comparable successes in explaining the

610   data. It is highly possible that several models are representative of the inter-event time over the two periods of time. In

611   this study, the number of data available is likely too small to allow for a robust model selection. Moreover, it is unclear

612   whether the probing is effective for characteristic earthquakes on a single fault or rather (and more likely) large

613   earthquakes in a wider zone. If the latter option is correct, both the Weibull and the gamma laws could be considered as

614   reasonable models, as they are generally seen as good models for recurrence and inter-occurrence times.

→ but you attribute your deposits to local events?

6 Conclusions

616   The multiproxy approach applied to Lake Aiguebelette deep basin sequences allowed the identification of a total of 55 event

617   layers during Holocene. Among them, eleven are undoubtfully homogenites or turbidite-homogenites (≥ 0.5 cm) located

618   in the top 250 cm of sediment which covers the period of the historical seismic catalogs. Based on visual observations,

619   grain-size, geochemical and AMS foliation data, these event layers are interpreted as seismically induced. A robust age-

620   depth model based on short-lived radionuclides, radiocarbon and palaeomagnetic data constraints their depositional ages

621   and allows a correlation with earthquakes archived in the seismic catalogs SisFrance and F-CAT.

622   Based on the ESTI (earthquake sensitivity threshold index) method, one historical earthquake is likely to have been

623   archived in the Lake Aiguebelette deep basin sequence, but it could correspond to either the 1784 or 1822 CE earthquake.

624   The ESTI method does not allow deciphering which of these two earthquakes triggered the deposition of the event layer

625   dated between 1760 and 1824 yr cal CE.

626   Complementary to the ESTI method, the calculation of PSA values for historical seismic events as a function of the

627   *hypocentral ?* epicentral distance to Lake Aiguebelette shows that it is more sensitive to local than to regional earthquakes. The Lake

628   Aiguebelette seems to be more sensitive to high frequencies, and thus the 1784 CE earthquake can be favoured as the

629   triggering event as supported by varves chemical analyses at the base and top of the event layer.

630   The thickness and frequency of event layers vary through time and 3 periods are evidenced. From -9890 to -2000 yr cal

631   CE, 21 event layers ≥ 0.5 cm are observed leading to a return period of 376 years

632   From -2000 CE to 0 yr cal CE no event layers ≥ 0.5 cm thick were archived (only 4 deposits < 0.5 cm-thick were

633   identified), probably due to a period of low-water level, as seen in other lakes worldwide (Osleger et al., 2009; Zhang et

634 al. 2014). From 0 to 2017 CE, 11 event layers ≥ 0.5 cm occurred; the corresponding return period is 183 years. A direct

635 link between return period and the sedimentation rate is not evidenced.

636 In the chronicle of the thickest event layers (thickness ≥ 4.5 cm) interpreted as seismically induced and covering the

637 Holocene a return period of ≈3000 to 4000 years (±500 years, based on the age-depth model uncertainties) is observed.

638 It is compatible with the previously calculated return period of 3435 years for an M=5 earthquake and a return period of

639 4857 years for a M ≥ 5.5 (in an area of 10 km radius around Lake Aiguebelette and for regional seismicity rates) estimated

640 by Banjan et al. (2023).

641 Based on the comparison of historical seismic event PSA values calculated with two GMPE laws, as a function of the

642 epicentral distance to the lake, it seems that the event layers archived in the sediment sequences could be generated by

643 local seismic events (epicentral distance < 50 km from Lake Aiguebelette).

644 The distribution of the number of event layers (identified independently of their thickness) archived in the Lake

645 Aiguebelette deep basin vs. the interval of time between each event layer deposition is compatible with statistical

646 distribution such as lognormal, Gamma, Weibull. Further interpretations based on this study need to be conducted

647 carefully as the sedimentation rate in Lake Aiguebelette deep basin has risen and might increase the sensitivity of the lake

648 sediment to record earthquake events over the last 2000 years. Further work on the horizontal-to-vertical (H/V) response

649 of background noise spectral ratios measured in Lake Aiguebelette would help discriminate whether the site is more prone

650 to amplify high or low frequencies.

651

7 Competing interests

653 The contact author has declared that none of the authors has any competing interests.

8 Acknowledgements

655

667   **References**

668   Abaimov, S. G., Turcotte, D. L., Shcherbakov, R., Rundle, J. B., Yakovlev, G., Goltz, C., and Newman, W. I.:

669   Earthquakes: recurrence and interoccurrence times, Earthquakes: Simulations, Sources and Tsunamis, 777, 777-795,

670   2008.

671

672   Ambraseys, N. N., and Finkel, C. F.: Long-term seismicity of Istanbul and of the Marmara Sea region, Terra Nova, 3,

673   527-539, 1991.

674

675   Appleby, P. G., Richardson, N., and Nolan, P. J.: 241Am dating of lake sediments, Hydrobiologia, 214, 35-42, 1991.

676

677   Avşar, U., Jónsson, S., Avşar, Ö., and Schmidt, S.: Earthquake-induced soft-sediment deformations and seismically

678   amplified erosion rates recorded in varved sediments of Köyceğiz Lake (SW Turkey), Journal of Geophysical Research:

679   Solid Earth, 121, 4767-4779, 2016.

680

681   Baize, S., Cushing, M., Lemeille, F., Gelis, C., Texier, D., Nicoud, G., and Schwenninger, J. L.: Contribution to the

682   seismic hazard assessment of a slow active fault, the Vuache fault in the southern Molasse basin (France), Bulletin de la

683   Société géologique de France, 182, 347-365, 2011.

684

685   Bajard, M., Sabatier, P., David, F., Develle, A. L., Reyss, J. L., Fanget, B., Arnaud, F.: Erosion record in Lake La Thuile

686   sediments (Prealps, France): Evidence of montane landscape dynamics throughout the Holocene, The Holocene, 26, 350-

687   364, 2016.

688

689 Banjan, M., Crouzet, C., Sabatier, P., Jomard, H., Bajard, M., Demory, F., Messager, E.: Did the Younger Dryas to
690 Holocene climate transition favour high seismicity rates in the north-western Alps?, Sedimentology, 70, 538-568, 2023.
691

692 Beck, C., Manalt, F., Chapron, E., Van Rensbergen, P., and De Batist, M.: Enhanced seismicity in the early post-glacial
693 period: evidence from the post-Würm sediments of Lake Annecy, northwestern Alps, Journal of Geodynamics, 22, 155-
694 171, 1996.
695

696 Beck, C., de Lépinay, B. M., Schneider, J. L., Cremer, M., Çağatay, N., Wendenbaum, E., Jaouen, A.: Late Quaternary
697 co-seismic sedimentation in the Sea of Marmara's deep basins, Sedimentary Geology, 199, 65-89, 2007.
698

699 Beck, C.: Late Quaternary lacustrine paleo-seismic archives in north-western Alps: Examples of earthquake-origin
700 assessment of sedimentary disturbances, Earth-Science Reviews, 96, 327-344, 2009.
701

702 Bellwald, B., Nigg, V., Fabbri, S. C., Becker, L. W., Gilli, A., Anselmetti, F. S.: Holocene seismic activity in south-
703 eastern Switzerland: Evidence from the sedimentary record of Lake Silvaplana, Sedimentology, 71, 116-151, 2024.
704

705 Berlioz, J.: L'effondrement du Mont Granier en Savoie (fin 1248), Le monde alpin et rhodanien, 15, 7-68, 1987.
706

707 Billaud, Y. and Lachenal, T.: Les palafittes des lacs savoyards, Actes de la séance de la Société préhistorique française
708 d'Agde, 47-65, 2017.
709

710 Blaauw, M.: Methods and code for 'classical'age-modelling of radiocarbon sequences, Quaternary geochronology, 5,
711 512-518, 2010.
712

713 Bruel, R. and Sabatier, P.: serac: an R package for ShortlivEd RAdionuclide chronology of recent sediment cores, Journal
714 of Environmental Radioactivity, 225, 106449, 2020.
715

716 Campos, C., Beck, C., Crouzet, C., Demory, F., Van Welden, A., and Eris, K.: Deciphering hemipelagites from
717 homogenites through anisotropy of magnetic susceptibility. Paleoseismic implications (Sea of Marmara and Gulf of
718 Corinth), Sedimentary Geology, 292, 1-14, 2013.
719

720   Cara, M., Cansi, Y., Schlupp, A., Arroucau, P., Béthoux, N., Beucler, E., Van Der Woerd, K.: SI-Hex: a new catalogue
721   of instrumental seismicity for metropolitan France, Bulletin de la Société Géologique de France, 186, 3-19, 2015.
722
723   Carrillo, E., Beck, C., Audemard, F. A., Moreno, E., and Ollarves, R.: Disentangling late Quaternary climatic and seismo-
724   tectonic controls on Lake Mucubají sedimentation (Mérida Andes, Venezuela), Palaeogeography, Palaeoclimatology,
725   Palaeoecology, 259, 284-300, 2008.
726
727   Corral, Á.: Long-term clustering, scaling, and universality in the temporal occurrence of earthquakes, Physical Review
728   Letters, 92, 108501, 2004.
729
730   Courboulex, F., Mercerat, E. D., Deschamps, A., Migeon, S., Baques, M., Larroque, C., Hello, Y.: Strong site effect
731   revealed by a new broadband seismometer on the continental shelf offshore nice airport (southeastern france), Pure and
732   Applied Geophysics, 177, 3205-3224, 2020.
733
734   Chapron, E., Beck, C., Pourchet, M., Deconinck, J. F.: 1822 earthquake-triggered homogenite in Lake Le Bourget (NW
735   Alps), Terra Nova, 11, 86-92, 1999.
736
737   Chapron, E.: Contrôles climatique et sismo-tectonique de la sédimentation lacustre dans l'avant pays alpin (Lac du
738   Bourget) durant le quaternaire récent. (Alpes françaises), Université de Lille 1, 1999.
739
740   Chapron, E., Simonneau, A., Ledoux, G., Arnaud, F., Lajeunesse, P., Albéric, P.: French Alpine Foreland Holocene
741   paleoseismicity revealed by coeval mass wasting deposits in glacial lakes, In Submarine Mass Movements and their
742   Consequences: 7th International Symposium, Springer International Publishing, 341-349, 2016.
743
744   Crouzet, C., Wilhelm, B., Sabatier, P., Demory, F., Thouveny, N., Pignol, C., Arnaud, F.: Palaeomagnetism for
745   chronologies of recent Alpine lake sediments: successes and limits, Journal of Paleolimnology, 62, 259-278, 2019a.
746
747   Crouzet, C., Wilhelm, B., Sabatier, P., Demory, F.: Magnetic characterization of instantaneous sedimentary deposits:
748   examples from alpine lakes, In Geophysical Research Abstracts, 21, 2019b.
749

750 Daxer, C., Huang, J. J. S., Weginger, S., Hilbe, M., Strasser, M., Moernaut, J.: Validation of seismic hazard curves using
751 a calibrated 14 ka lacustrine record in the Eastern Alps, Austria, Scientific reports, 12, 19943, 2022.

752

753 De Gelder, G., Doan, M. L., Beck, C., Carlut, J., Seibert, C., Feuillet, N., Gawthorpe, R. L.: Multi-scale and multi-
754 parametric analysis of Late Quaternary event deposits within the active Corinth rift (Greece), Sedimentology, 69, 1573-
755 1598, 2022.

756

757 de La Taille, C., Jouanne, F., Crouzet, C., Beck, C., Jomard, H., De Rycker, K., Van Daele, M.: Impact of active faulting
758 on the post LGM infill of Le Bourget Lake (western Alps, France), Tectonophysics, 664, 31-49, 2015.

759

760 Demory, F., Uehara, M., Quesnel, Y., Rochette, P., Romey, C., Tachikawa, K., Andrieu-Ponel, V.: A new high-resolution
761 magnetic scanner for sedimentary sections, Geochemistry, Geophysics, Geosystems, 20, 3186-3200, 2019.

762

763 Ergin, M., Özalaybey, S., Aktar, M., Yalcin, M. N.: Site amplification at Avcılar, Istanbul, Tectonophysics, 391, 335-
764 346, 2004.

765

766 Fudral, S., Nicoud, G., Paillet, A., Faivre, P., Laslaz, L., Menard, G., Tritenne, D., Rey, P.J., Mani, C.: Notice explicative
767 et Carte géol. France (1/50 000), feuille Chambéry, BRGM edition, Orléans, (In Press).

768

769 Gastineau, R., De Sigoyer, J., Sabatier, P., Fabbri, S. C., Anselmetti, F. S., Develle, A. L., Gebhardt, A. C.: Active
770 subaquatic fault segments in Lake Iznik along the middle strand of the North Anatolian Fault, NW Turkey, Tectonics, 40,
771 e2020TC006404, 2021.

772

773 Giguet-Covex, C., Arnaud, F., Poulenard, J., Enters, D., Reyss, J. L., Millet, L., Vidal, O.: Sedimentological and
774 geochemical records of past trophic state and hypolimnetic anoxia in large, hard-water Lake Bourget, French Alps, Journal
775 of Paleolimnology, 43, 171-190, 2010.

776

777 Hasumi, T., Akimoto, T., and Aizawa, Y.: The Weibull–log Weibull distribution for interoccurrence times of earthquakes,
778 Physica A: Statistical Mechanics and its Applications, 388, 491-498, 2009.

779

780   Jomard, H., Scotti, O., Auclair, S., Dominique, P., Manchuel, K., Sicilia, D.: The SISFRANCE database of historical

781   seismicity. State of the art and perspectives, Comptes Rendus. Géoscience, 353, 1-24, 2021.

782

783   Jomard, H., Cushing, E. M., Palumbo, L., Baize, S., David, C., Chartier, T.: Transposing an active fault database into a

784   seismic hazard fault model for nuclear facilities–Part 1: Building a database of potentially active faults (BDFA) for

785   metropolitan France, Natural Hazards and Earth System Sciences, 17, 1573-1584, 2017.

786

787   Korte, M., Constable, C., Donadini, F., Holme, R.: Reconstructing the Holocene geomagnetic field, Earth and Planetary

788   Science Letters, 312, 497-505, 2011.

789

790   Kremer, K., Hilbe, M., Simpson, G., Decrouy, L., Wildi, W., Girardclos, S.: Reconstructing 4000 years of mass movement

791   and tsunami history in a deep peri-Alpine lake (Lake Geneva, France-Switzerland), Sedimentology, 62, 1305-1327, 2015.

792

793   Kremer, K., Wirth, S. B., Reusch, A., Fäh, D., Bellwald, B., Anselmetti, F. S., Strasser, M.: Lake-sediment based

794   paleoseismology: Limitations and perspectives from the Swiss Alps, Quaternary Science Reviews, 168, 1-18, 2017.

795

796   Lurcock, P. C., and Wilson, G. S.: PuffinPlot: A versatile, user-friendly program for paleomagnetic analysis,

797   Geochemistry, Geophysics, Geosystems, 13, 2012.

798

799   Manchuel, K., Traversa, P., Baumont, D., Cara, M., Nayman, E., Durouchoux, C.: The French seismic CATalogue

800   (FCAT-17), Bulletin of Earthquake Engineering, 16, 2227-2251, 2018.

801

802   Matthews, M. V., Ellsworth, W. L., Reasenberg, P. A.: A Brownian model for recurrent earthquakes, Bulletin of the

803   Seismological Society of America, 92, 2233-2250, 2002.

804

805   Maufroy, E., Chaljub, E., Hollender, F., Kristek, J., Moczo, P., Klin, P., Bard, P. Y.: Earthquake ground motion in the

806   Mygdonian basin, Greece: The E2VP verification and validation of 3D numerical simulation up to 4 Hz, Bulletin of the

807   Seismological Society of America, 105, 1398-1418, 2015.

808

809   Messager, E., Giguet-Covex, C., Doyen, E., Etienne, D., Gielly, L., Sabatier, P., Arnaud, F.: Two millennia of complexity
810   and variability in a perialpine socioecological system (Savoie, France): the contribution of palynology and sedaDNA
811   analysis, Frontiers in Ecology and Evolution, 10, 866781, 2022.

812

813   Moernaut, J., Van Daele, M. E., Vandoorne, W., Urrutia, R., Pino Quivira, M., De Batist, M. A.: The sedimentary imprint
814   of the Mw 8.8 Maule earthquake (27th February 2010) in 10 different lakes between Santiago and Valdivia, South-Central
815   Chile, In AGU Fall Meeting Abstracts, S21A-2140, 2011.

816

817   Moernaut, J., Daele, M. V., Heirman, K., Fontijn, K., Strasser, M., Pino, M., De Batist, M.: Lacustrine turbidites as a tool
818   for quantitative earthquake reconstruction: New evidence for a variable rupture mode in south central Chile, Journal of
819   Geophysical Research: Solid Earth, 119, 1607-1633, 2014.

820

821   Moernaut, J., Van Daele, M., Fontijn, K., Heirman, K., Kempf, P., Pino, M., De Batist, M.: Larger earthquakes recur
822   more periodically: New insights in the megathrust earthquake cycle from lacustrine turbidite records in south-central
823   Chile, Earth and Planetary Science Letters, 481, 9-19, 2018.

824

825   Moernaut, J.: Time-dependent recurrence of strong earthquake shaking near plate boundaries: A lake sediment
826   perspective, Earth-Science Reviews, 210, 103344, 2020.

827

828   Monecke, K., Anselmetti, F. S., Becker, A., Sturm, M., Giardini, D.: The record of historic earthquakes in lake sediments
829   of Central Switzerland, Tectonophysics, 394, 21-40, 2004.

830

831   Nakajima, T., and Kanai, Y.: Sedimentary features of seismoturbidites triggered by the 1983 and older historical
832   earthquakes in the eastern margin of the Japan Sea, Sedimentary Geology, 135, 1-19, 2000.

833

834   Nicoud, G., Dzikowski, M., Paillet, A., Ghoreychi, R., Emeric, P., Chignoli, M.: Données nouvelles sur la nature et
835   l'extension du glissement historique du Granier, Documents de l'Académie de Savoie, deuxième série, 35-54, 1999.

836

837   Nishenko, S. P., and Buland, R.: A generic recurrence interval distribution for earthquake forecasting, Bulletin of the
838   Seismological Society of America, 77, 1382-1399, 1987.

839

840   Nomade, J.: Chronologie et sédimentologie du remplissage du lac d'Annecy depuis le Tardiglaciaire: Implications
841   paléoclimatologiques et paléohydrologiques, Université Joseph-Fourier-Grenoble I, 187p, 2005.

843   Nomade, J., Chapron, E., Desmet, M., Reyss, J. L., Arnaud, F., Lignier, V.: Reconstructing historical seismicity from lake
844   sediments (Lake Laffrey, western Alps, France), Terra Nova, 17, 350-357, 2005.

846   Osleger, D. A., Heyvaert, A. C., Stoner, J. S., Verosub, K. L.: Lacustrine turbidites as indicators of Holocene storminess
847   and climate: Lake Tahoe, California and Nevada, Journal of Paleolimnology, 42, 103-122, 2009.

849   Passega, R.: Grain size representation by CM patterns as a geologic tool, Journal of Sedimentary Research, 34, 830-847,
850   1964.

852   Petersen, J., Wilhelm, B., Revel, M., Rolland, Y., Crouzet, C., Arnaud, F., Magand, O.: Sediments of Lake Vens (SW
853   European Alps, France) record large-magnitude earthquake events, Journal of paleolimnology, 51, 343-355, 2014.

855   Pétrequin, P. and Bailly, M.: Lake-dwelling research in France, Living on the Lake in Prehistoric Europe: 150 Years of
856   Lake-Dwelling Research, 36, 2004.

858   Praet, N., Van Daele, M., Collart, T., Moernaut, J., Vandekerkhove, E., Kempf, P., De Batist, M.: Turbidite stratigraphy
859   in proglacial lakes: Deciphering trigger mechanisms using a statistical approach, Sedimentology, 67, 2332-2359, 2020.

861   Rapuc, W., Sabatier, P., Andrič, M., Crouzet, C., Arnaud, F., Chapron, E., Von Grafenstein, U.: 6600 years of earthquake
862   record in the Julian Alps (Lake Bohinj, Slovenia), Sedimentology, 65, 1777-1799, 2018.

864   Rapuc, W., Sabatier, P., Arnaud, F., Palumbo, A., Develle, A. L., Reyss, J. L., von Grafenstein, U.: Holocene-long record
865   of flood frequency in the Southern Alps (Lake Iseo, Italy) under human and climate forcing, Global and Planetary Change,
866   175, 160-172, 2019.

868   Reimer, P. J., Austin, W. E., Bard, E., Bayliss, A., Blackwell, P. G., Ramsey, C. B., Talamo, S.: The IntCal20 Northern
869   Hemisphere radiocarbon age calibration curve (0–55 cal kBP), Radiocarbon, 62, 725-757, 2020.

870

871   Rovida, A., Antonucci, A., and Locati, M.: The European Preinstrumental Earthquake Catalogue EPICA, the 1000–1899

872   catalogue for the European Seismic Hazard Model 2020, Earth System Science Data, 14, 5213-5231, 2022.

873

874   Sabatier, P., Moernaut, J., Bertrand, S., Van Daele, M., Kremer, K., Chaumillon, E., Arnaud, F.: A Review of Event

875   Deposits in Lake Sediments, Quaternary, 5, 34, 2022.

876

877   Schnellmann, M., Anselmetti, F. S., Giardini, D., McKenzie, J. A., Ward, S. N.: Prehistoric earthquake history revealed

878   by lacustrine slump deposits, Geology, 30, 1131-1134, 2002.

879

880   Scotti, O., Baumont, D., Quenet, G., Levret, A.: The French macroseismic database SISFRANCE: objectives, results and

881   perspectives, Annals of geophysics, 2004.

882

883   Strasser, M., Anselmetti, F. S., Fäh, D., Giardini, D., Schnellmann, M.: Magnitudes and source areas of large prehistoric

884   northern Alpine earthquakes revealed by slope failures in lakes, Geology, 34, 1005-1008, 2006.

885

886   Strasser, M., Monecke, K., Schnellmann, M., Anselmetti, F. S.: Lake sediments as natural seismographs: A compiled

887   record of Late Quaternary earthquakes in Central Switzerland and its implication for Alpine deformation, Sedimentology,

888   60, 319-341, 2013.

889

890   Van Daele, M., Moernaut, J., Doom, L., Boes, E., Fontijn, K., Heirman, K., De Batist, M.: A comparison of the

891   sedimentary records of the 1960 and 2010 great Chilean earthquakes in 17 lakes: Implications for quantitative lacustrine

892   palaeoseismology, Sedimentology, 62, 1466-1496, 2015.

893

894   Weltje, G. J., Bloemsma, M. R., Tjallingii, R., Heslop, D., Röhl, U., Croudace, I. W.: Prediction of geochemical

895   composition from XRF core scanner data: a new multivariate approach including automatic selection of calibration

896   samples and quantification of uncertainties, Micro-XRF Studies of Sediment Cores: Applications of a non-destructive

897   tool for the environmental sciences, 507-534, 2015.

898

899   Wilhelm, B., Arnaud, F., Sabatier, P., Magand, O., Chapron, E., Courp, T., Delannoy, J. J.: Palaeoflood activity and

900   climate change over the last 1400 years recorded by lake sediments in the north-west European Alps, Journal of

901   Quaternary Science, 28, 189-199, 2013.

Natural Hazards
and Earth System
Sciences
Discussions

902

903 Wilhelm, B., Nomade, J., Crouzet, C., Litty, C., Sabatier,

904

905 P., Belle, S., Anselmetti, F. S.: Quantified sensitivity of small lake sediments to record historic earthquakes: Implications

906 for paleoseismology, Journal of Geophysical Research: Earth Surface, 121, 2-16, 2016.

907

908 Williams, R. T., Davis, J. R., Goodwin, L. B.: Do large earthquakes occur at regular intervals through time? A perspective

909 from the geologic record, Geophysical Research Letters, 46, 8074-8081, 2019.

910

911 Wirth, S. B., Gilli, A., Simonneau, A., Ariztegui, D., Vannière, B., Glur, L., Anselmetti, F. S.: A 2000 year long seasonal

912 record of floods in the southern European Alps, Geophysical Research Letters, 40, 4025-4029, 2013.

913

914 Yakupoğlu N., Henry P., Uçarkuş G., Eriş K., Demory F., Crouzet C., Çağatay N.: Factors Affecting Deposition of

915 Turbidite-Homogenite Units in Kumburgaz Basin, Sea of Marmara: Critical Assessment of Their Use in Submarine

916 Paleoseismology, Marine geology, 452, 2022.

917

918 Zhang, X., Scholz, C. A., Hecky, R. E., Wood, D. A., Zal, H. J., Ebinger, C. J.: Climatic control of the late Quaternary

919 turbidite sedimentology of Lake Kivu, East Africa: Implications for deep mixing and geologic hazards, Geology, 42, 811-

920 814, 2014.

921

922 Zijderveld, J.D.A.: A.C. demagnetization: analysis of results, In: Methods in Paleomagnetism, Elsevier, Amsterdam, 254-

923 286, 1967.

924

925 Zöller, G., Hainzl, S., Holschneider, M.: Recurrent large earthquakes in a fault region: What can be inferred from small

926 and intermediate events?, Bulletin of the Seismological Society of America, 98, 2641-2651, 2008.

927

928 Zöller, G.: A statistical model for earthquake recurrence based on the assimilation of paleoseismicity, historic seismicity,

929 and instrumental seismicity, Journal of Geophysical Research: Solid Earth, 123, 4906-4921, 2018.